Low-Energy Measurements of the Weak Mixing Angle

K.S. Kumar,[1] Sonny Mantry,[2] W.J. Marciano,[3] and P.A. Souder[4]

[1]Department of Physics, University of Massachusetts, Amherst, Massachusetts 01003; email: kkumar@physics.umass.edu

[2]Argonne National Laboratory and Department of Physics and Astronomy, Northwestern University, Evanston, Illinois 60208

[3]Physics Department, Brookhaven National Laboratory, Upton, New York 11973

[4]Physics Department, Syracuse University, Syracuse, New York 13244

Annu. Rev. Nucl. Part. Sci. 2013. 63:237–67

First published online as a Review in Advance on July 10, 2013

The *Annual Review of Nuclear and Particle Science* is online at nucl.annualreviews.org

This article's doi: 10.1146/annurev-nucl-102212-170556

Keywords

weak neutral currents, weak mixing angle, precision tests of the Standard Model, electroweak radiative corrections

Abstract

We review the status of precision measurements of weak neutral-current interactions, mediated by the Z^0 boson, at $Q^2 \ll M_Z^2$. They can be used to extract values for the weak mixing angle $\sin^2\theta_W$, a fundamental parameter of the $SU(2)_L \times U(1)_Y$ electroweak sector of the Standard Model. Apart from providing a comprehensive test of the electroweak theory at the quantum-loop level, such measurements allow indirect access to New Physics effects at and beyond the TeV scale. After providing a theoretical introduction and a brief overview of the three most precise low-Q^2 weak mixing angle determinations, we describe the ongoing experimental program and prospects for future, more sensitive studies. We also compare the sensitivities of planned and proposed measurements with physics beyond the Standard Model.

Contents

1. INTRODUCTION

1.1. Historical Context

In 1961, Glashow (1) introduced an $SU(2)_L \times U(1)_Y$ symmetry that would form the basis for electroweak unification. In modern terminology, it contained four spin-1 vector bosons, W_μ^+, W_μ^0, W_μ^-, and B_μ^0, along with two independent couplings, g and g'. Mixing gave rise to a massless photon and its orthogonal massive partner, now known as the Z^0 boson:

$$\begin{aligned} A_\mu &= B_\mu^0 \cos\theta_W + W_\mu^0 \sin\theta_W, \\ Z_\mu &= W_\mu^0 \cos\theta_W - B_\mu^0 \sin\theta_W. \end{aligned} \qquad 1.$$

That formalism marked the birth of the weak mixing angle, θ_W, defined by $\tan\theta_W = g'/g$ or, in terms of the electromagnetic coupling $e = gg'/\sqrt{g^2 + g'^2}$, $\sin\theta_W = e/g$. Particle masses were arbitrarily put in by hand and were unrelated to other parameters in the theory.

In 1967, Weinberg (2) appended the Higgs mechanism (3–7) to $SU(2)_L \times U(1)_Y$ electroweak gauge unification via a complex, spin-0 scalar doublet whose vacuum expectation value spontaneously broke the gauge symmetry to $U(1)_{EM}$ and gave rise to $W^{\pm}$ and Z^0 boson masses related by $m_W = m_Z \cos\theta_W$. It also led to a physical spin-0 Higgs boson with arbitrary mass, m_H. As an added bonus, the Higgs boson that originally accommodated charged lepton masses later proved well suited to the inclusion of quark masses and mixing (8), including *CP* (charge–parity) violation. Weinberg speculated that the theory might be renormalizable and that weak neutral-current effects, mediated by the Z^0 boson, should be observed in neutrino scattering.

In 1971, 't Hooft (9) proved renormalizability for gauge theories with spontaneous symmetry breaking, and weak neutral currents were discovered in 1973 (10). Together, these developments confirmed the consistency and basic ingredients of electroweak unification.

The combination $SU(2)_L \times U(1)_Y$ gauge invariance + Higgs doublet + renormalizability led to natural relationships among the bare (unrenormalized) gauge boson masses and couplings (11):

$$\sin^2\theta_W^0 = e_0^2/g_0^2 = 1 - m_W^{0^2}/m_Z^{0^2}. \qquad 2.$$

Those relations are respected by the renormalized parameters, up to finite calculable radiative corrections (11, 12). Such corrections, discussed in Section 1.2, test the theory at its quantum-loop level and probe for potential New Physics effects.

By the mid 1970s, the basic features of $SU(2)_L \times U(1)_Y$ electroweak unification had nearly been established. The quark model (including charm) and its associated strong $SU(3)_c$ color gauge interactions, quantum chromodynamics (QCD), had been elegantly incorporated, while weak neutral-current effects continued to be observed at approximately the predicted rate. However, it was not clear that the model's specific weak neutral-current interaction (2),

$$\frac{g}{\cos\theta_W} Z_\mu \bar{f}\gamma^\mu (T_{3f} - 2Q_f \sin^2\theta_W - T_{3f}\gamma_5) f, \quad T_{3f} = \pm\frac{1}{2}, \qquad 3.$$

was correct. In particular, that interaction implied a small degree of parity violation throughout low-energy physics due to $\gamma - Z^0$ interference. Such effects were enhanced in atoms with a large number of protons (Z) and neutrons (N) by the coherent weak charge that quantifies the Z^0–nucleus vector coupling (13)

$$Q_W(\mathrm{Z},\mathrm{N}) = \mathrm{Z}(1 - 4\sin^2\theta_W) - \mathrm{N}. \qquad 4.$$

Unfortunately, the early efforts to measure atomic parity violation (APV) by use of ^{209}Bi failed to observe the expected effect (14, 15) and cast some doubt on the specific form of Equation 3. [Later studies with ^{209}Bi, ^{205}Tl, and ^{133}Cs observed parity violation at the expected level (16–19).]

In 1978, the now-classic E122 experiment at SLAC, led by Prescott and colleagues (20), searched for helicity dependence in the inclusive cross section $\sigma_{R(L)}$ for deep-inelastic scattering (DIS) of longitudinally polarized electrons off unpolarized ^{2}H. Defining a parity-violating asymmetry (A_{PV}) as

$$A_{PV} \equiv \frac{\sigma_R - \sigma_L}{\sigma_R + \sigma_L}, \qquad 5.$$

the measured value, $A_{PV} \simeq (-1.52 \pm 0.26) \times 10^{-4}$, confirmed the predicted form in Equation 3 and determined $\sin^2\theta_W$ with relatively good precision ($\pm 10\%$): $\sin^2\theta_W \simeq 0.22(2)$.

That milestone experiment established $SU(2)_L \times U(1)_Y$ as the structure of electroweak interactions in the Standard Model (SM). In addition, the measured value of $\sin^2\theta_W$ lent support to grand unified theories (GUTs) (21, 22), such as $SU(5)$, $SO(10)$, and so on. Assuming a "great desert"—that is, no New Physics between the SM and the unification scale $m_X \simeq 10^{15}$ GeV—those theories

predicted, at one loop ($\alpha = e^2/4\pi \simeq 1/137$) (23), that

$$\sin^2\theta_W \approx \frac{3}{8}\left[1 - \frac{109\alpha}{18\pi}\ln\frac{m_X}{m_W}\right] \simeq 0.21 \quad \text{[one-loop minimal } SU(5)\text{]}, \qquad 6.$$

in accord with the SLAC E122 value. [That simplistic scheme was, however, later ruled out by its failure to accommodate complete coupling unification and proton decay ($p \to e^+\pi^0$) constraints. Nevertheless, GUTs continue to be an interesting paradigm; they are still used to advance low-energy supersymmetry (24) as a unifying desert ingredient.]

1.2. The Weak Mixing Angle and Quantum Corrections

In the 1980s, it became clear that to rigorously test the SM and GUTs at the level of their quantum corrections, $\sin^2\theta_W$ and the other electroweak parameters in Equation 2 (m_W; m_Z; α; and the Fermi constant, $G_F = g^2/4\sqrt{2}m_W^2$) would have to be determined with very high precision (25, 26): $\mathcal{O}(\pm 0.1\%)$ or better. Some were already known at a level orders of magnitude better than needed; currently (27, 28), $\alpha^{-1} = 137.035999173(35)$ and $G_F = 1.1663787(6) \times 10^{-5}$ GeV^{-2}. In the case of vector boson masses, LEP and the Tevatron later made great progress (29); they found $m_Z = 91.1876(21)$ GeV and $m_W = 80.385(15)$ GeV.

For $\sin^2\theta_W$, an important issue was the requirement of a rigorous definition of the renormalized weak mixing angle for precision experimental extraction. At first, the on-shell definition (30, 31)

$$\sin^2\theta_W \equiv 1 - m_W^2/m_Z^2 \qquad 7.$$

was popular. However, after the top quark mass was found to be large [the currently accepted value is $m_t = 173.3(8)$ GeV], the on-shell definition was largely abandoned because its use induced large, misleading $\mathcal{O}(\alpha m_t^2/m_W^2)$ radiative corrections to weak neutral-current processes. Instead, at LEP, it became common practice to employ an effective $\sin^2\theta_W^{\text{eff}}$, defined by the $Z^0\mu^+\mu^-$ coupling at the Z^0 pole. The only drawback was the complexity of finite, renormalized counterterms required for non–Z^0 pole applications.

For computational convenience and comparison with GUT predictions, it was easier to employ the more theoretically motivated (but unphysical) $\overline{\text{MS}}$ (modified minimal subtraction) prescription (originally introduced for QCD) (25, 32)

$$\sin^2\theta_W(\mu)_{\overline{\text{MS}}} = e^2(\mu)_{\overline{\text{MS}}}/g^2(\mu)_{\overline{\text{MS}}}, \qquad 8.$$

with an arbitrary sliding mass scale μ. Numerically, it is related to $\sin^2\theta_W^{\text{eff}}$, used at LEP, by (33)

$$\sin^2\theta_W(m_Z)_{\overline{\text{MS}}} = \sin^2\theta_W^{\text{eff}} - 0.00028, \qquad 9.$$

making translation between the two schemes straightforward.

Currently, the two best determinations of $\sin^2\theta_W(m_Z)_{\overline{\text{MS}}}$ come from the right–left Z pole production asymmetry A_{RL}, measured at SLAC (34),

$$\sin^2\theta_W(m_Z)_{\overline{\text{MS}}} = 0.23070(26) \quad A_{RL}, \qquad 10.$$

and from the $Z \to b\bar{b}$ forward-backward asymmetry $A_{\text{FB}}(b\bar{b})$, measured at LEP1 (35),

$$\sin^2\theta_W(m_Z)_{\overline{\text{MS}}} = 0.23193(29) \qquad A_{\text{FB}}(b\bar{b}). \qquad 11.$$

Unfortunately, these values disagree by 3.2 σ. Even the overall LEP1 average, including lepton forward–backward asymmetries and τ polarization, $\sin^2\theta_W(m_Z)_{\overline{\text{MS}}} = 0.23161(21)$, is somewhat high in comparison to Equation 10. Nevertheless, all Z^0 pole measurements are usually averaged

to give

$$\sin^2\theta_W(m_Z)_{\overline{\rm MS}} = 0.23125(16) \quad Z \text{ pole average} \qquad 12.$$

for comparison with other precision studies. The spread in the most precisely measured values of $\sin^2\theta_W(m_Z)_{\overline{\rm MS}}$ remains, however, somewhat troubling and needs to be resolved, as underscored by an example of their different implications (discussed toward the end of this subsection).

The exquisite precision achieved in the measurements of m_Z, m_W, and $\sin^2\theta_W$ allows for important tests of the electroweak theory at the level of quantum loops. In the process of renormalization, finite radiative corrections upset the natural relations of Equation 2. The fractional deviation has historically (30, 31) been termed Δr. It arises primarily from fermion and boson vacuum polarizations (including those involving top quarks and SM bosons that are heavier than the energy scales of various measurements) but could also receive contributions from other indirect effects of even-higher-mass-scale New Physics. Conventionally, three different quantities have been used to parameterize the deviations in the finite radiative corrections from zero (30, 31, 36, 37, 38, 39) because of their distinctly different dependencies on m_t, m_H, and New Physics:

$$\begin{aligned}(\Delta r)^{\rm exp} &= 1 - \left[\pi\alpha/\{\sqrt{2}G_{\rm F}m_W^2(1 - m_W^2/m_Z^2)\}\right] = 0.0350(9),\\ (\Delta r)^{\rm SM} &= 0.0364(3) + 3.4\times10^{-3}\ln(m_H/126\,{\rm GeV}),\end{aligned} \qquad 13.$$

$$\begin{aligned}(\Delta\hat{r})^{\rm exp} &= 1 - \left[2\sqrt{2}\pi\alpha/\{G_F m_Z^2\sin^2 2\theta_W(m_Z)_{\overline{\rm MS}}\}\right] = 0.0598(5),\\ (\Delta\hat{r})^{\rm SM} &= 0.0598(2) + 1.4\times10^{-3}\ln(m_H/126\,{\rm GeV}),\end{aligned} \qquad 14.$$

$$\begin{aligned}(\Delta r_{\overline{\rm MS}})^{\rm exp} &= 1 - \left[\pi\alpha/\{\sqrt{2}G_{\rm F}m_W^2\sin^2\theta_W(m_Z)_{\overline{\rm MS}}\}\right] = 0.0699(7)(4),\\ (\Delta r_{\overline{\rm MS}})^{\rm SM} &= 0.0693(2) + 6.5\times10^{-4}\ln(m_H/126\,{\rm GeV}),\end{aligned} \qquad 15.$$

where the dependence of the first two corrections on m_H provide sensitivity to it, whereas $\Delta r_{\overline{\rm MS}}$ is less dependent on m_H. We emphasize that the values on the right (on the first line of each equation) are purely experimental determinations. Those on the second line of each equation incorporate detailed calculations of SM loop corrections (37; 38; 39; 40; 41, p. 48) (assuming no New Physics) and use experimental measurements of $\alpha_{\rm EM}$, $G_{\rm F}$, m_Z, and m_t as input. The theoretical predictions are dominated by a +7% shift due to fermion vacuum polarization effects that lead to the running of $\alpha_{\rm EM}$ from $\alpha(0) = 1/137$ to $\alpha(m_Z)_{\overline{\rm MS}} = 1/127.9$, but they also include important dependences on m_H and m_t. Also, note that we have normalized the predictions at $m_H = 126$ GeV, the tentative value of the new scalar resonance recently discovered at the Large Hadron Collider (LHC) (42, 43).

Alternatively, from the first two corrections one can obtain the predictions (Equations 13 and 14) $m_W = 80.362(6)$ GeV and $\sin^2\theta_W(m_Z)_{\overline{\rm MS}} = 0.23124(6)$ for $m_H = 126$ GeV, where the uncertainties are due to the errors in m_t and hadronic effects. [The errors are approximately doubled if one includes estimated uncertainties in uncalculated higher-order effects (44).] The agreement between those predictions and the corresponding world averages of current measurements constitutes a beautiful verification of the electroweak theory at the quantum-loop level and constrains many New Physics scenarios. If instead one takes the world averages for m_W and $\sin^2\theta_W$, one obtains $m_H = 97^{+24}_{-20}$ GeV, which agrees relatively well with the LHC finding, although somewhat low, but still leaves some room for New Physics.

The experimental determinations of m_W and $\sin^2\theta_W$ also provide a direct probe of New Physics through a test of the validity of the third $\Delta r_{\overline{\rm MS}}$ relation (Equation 15). For example, taking $m_H \simeq 126$ GeV but allowing for $N_{\rm D}$ heavy new chiral doublets ($N_{\rm D} = 4$ for a fourth generation) via $S = N_{\rm D}/6\pi$ or a heavy $W^{*\pm}$ excited W boson, comparison with experimental values leads to (45, 46)

$$\Delta r_{\overline{\rm MS}}(m_Z) = 0.0693(2) + 0.0085S + \left(\frac{m_W}{m_{W^*}}\right)^2 = 0.0699(8) \qquad 16.$$

or

$$S = 0.07(9) \rightarrow N_D \leq 4 \quad \text{(one-sided 95\%CL)},$$
$$m_{W^*} > 2.2 \text{ TeV} \quad \text{(one-sided 95\%CL)}. \qquad 17.$$

Such constraints appear to tightly restrict New Physics. However, they are quite dependent on the Z^0 pole average $\sin^2\theta_W(m_Z)_{\overline{\rm MS}}$ employed, as well as on the overall error. If instead one uses the $A_{\rm FB}(b\bar{b})$ value in Equation 11, it suggests that $S \approx 0.4$ or $N_D \simeq 6$–7, which is more in keeping with dynamical symmetry–breaking (technicolor) or fourth-generation scenarios. Additionally, in Equation 15, the larger (smaller) error is due to the uncertainty in $\sin^2\theta_W$ (m_W). This observation underscores the need for improved experimental determinations of $\sin^2\theta_W$, the topic of this review.

1.3. The Weak Mixing Angle at $Q^2 \ll M_Z^2$

What do low-energy determinations of $\sin^2\theta_W$ add to the above discussion? How do they complement the already precise Z^0 pole measurements? Currently, there are three low-Q^2 measurements of $\sin^2\theta_W$ at the $\pm 1\%$ level or better. They are reviewed in Section 2, where we include details and caveats associated with each extraction. Here, we summarize the results extrapolated to the m_Z scale for comparison with Z^0 pole measurements (47–49):

$$\sin^2\theta_W(m_Z)_{\overline{\rm MS}} = 0.2283(20) \quad \text{Cs APV at } \langle Q\rangle \simeq 2.4\,\text{MeV}, \qquad 18.$$

$$\sin^2\theta_W(m_Z)_{\overline{\rm MS}} = 0.2329(13) \quad \text{Møller } A_{\rm PV} \text{ at } \langle Q\rangle \simeq 160\,\text{MeV}, \qquad 19.$$

$$\sin^2\theta_W(m_Z)_{\overline{\rm MS}} = 0.2356(16) \quad \nu_\mu N \text{ at } \langle Q\rangle \simeq 5\,\text{GeV}. \qquad 20.$$

Those values are not directly competitive with Z^0 pole results. Even the average of Equations 18–20, $\sin^2\theta_W(m_Z)_{\overline{\rm MS}} = 0.2328(9)$ [i.e., $\mathcal{O}(\pm 0.4\%)$], lends little to the above discussion. However, as we discuss in Section 3, future polarized electron scattering asymmetries at low Q^2 are expected to reach similar precision to the best Z^0 pole measurements: $\mathcal{O}(\pm 0.1 - 0.2\%)$. At that level, they may help resolve differences between the SLAC and LEP1 results or may, as discussed below, find interesting new effects.

Apart from improved precision testing of the electroweak theory at the quantum-loop level, low-Q^2 measurements are sensitive to classes of New Physics effects to which Z^0 pole measurements are insensitive. The measurements in Equations 18–20 can already be used to constrain New Physics such as Z' bosons or general four-fermion contact interactions. Future, more precise experiments are expected to probe the 1–20-TeV scale, as described in Section 4. We also show how such experiments may be used to explore very weakly coupled low-mass-scale "dark boson" effects.

In addition, the low-Q^2 results are already testing the SM predicted running (25, 26, 32, 50–52) of $\sin^2\theta_W$ as a function of Q^2. The evolution of that quantity can be examined in the $\overline{\rm MS}$ framework of Equation 8 by using the $e(\mu)$ and $g(\mu)$ β functions. **Figure 1** illustrates the running, along with the three measurements with $\mu = \langle Q\rangle$ determined from each experiment's average momentum conditions (53). The only drawback to that formalism is that the unphysical $\overline{\rm MS}$ discontinuities at $\mu = \langle Q\rangle =$ particle masses. To circumvent that problem, it is useful to define a more physical running weak angle (50–52, 54),

$$\sin^2\theta_W(Q^2) = \kappa(Q^2)\sin^2\theta_W(m_Z)_{\overline{\rm MS}}, \qquad 21.$$

where $\kappa(Q^2)$ incorporates perturbative $\gamma - Z$ mixing through vacuum polarization and other, smaller corrections. This scenario is illustrated in **Figure 1**, normalized such that $\kappa(Q^2 = m_Z^2) \simeq 1.000$, whereas $\kappa(0)$ is $\sim$1.030. This 3% variation is particularly important for some low-Q^2

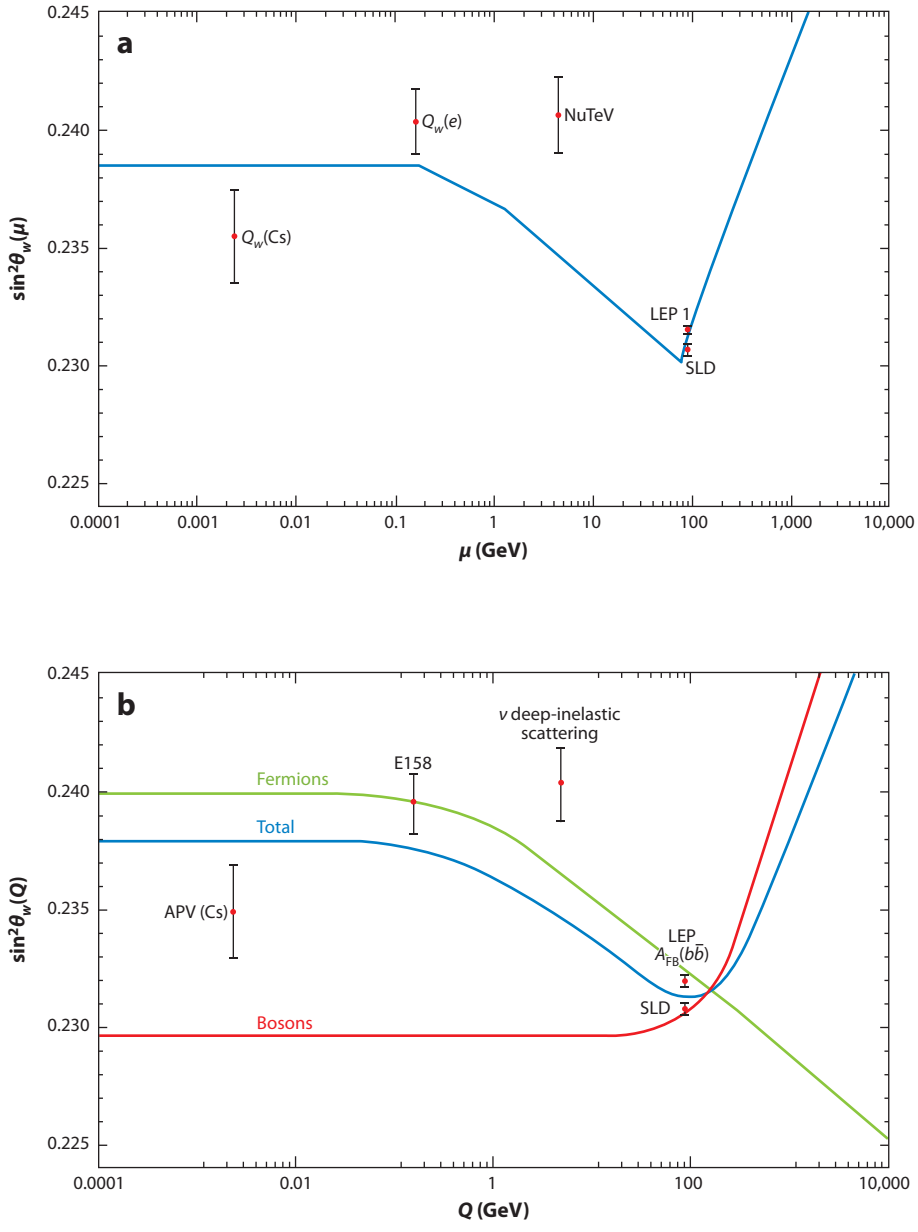

Figure 1

(*a*) $\sin^2\theta_W(\mu)_{\overline{\rm MS}}$ (29) with an updated atomic parity violation (APV) result. (*b*) $\sin^2\theta_W(Q^2)$, a one-loop calculation dominated by $\gamma - Z^0$ mixing (52). The red and green curves represent the boson and fermion contributions, respectively.

polarized electron scattering asymmetries proportional to $1 - 4\sin^2\theta_W(Q^2)$ (examples discussed in Section 3) that are very sensitive to small variations in $\sin^2\theta_W(Q^2)$. Indeed, the 3% shift in $\sin^2\theta_W$ results in a roughly 40% change in $1 - 4\sin^2\theta_W$ [$(0.075 \rightarrow 0.046)$ at $\langle Q\rangle \approx 0.1$ GeV].

Of course, to test the running of $\sin^2\theta_W(Q^2)$ and try to unveil New Physics requires confidence in the theoretical underpinnings of the various reactions studied. To that end, we examine in Section 5 the status of several theoretical issues, including hadronic uncertainties in $\kappa(0)$ and γZ^0 box diagrams. However, we emphasize that each experimental measurement should be compared with a calculation that is specific to the relevant experimental conditions, including complete one-loop and leading two-loop effects and estimates of hadronic contribution uncertainties. The latter are under control for measurements at very low Q^2 and high Q^2 but may require more careful studies at intermediate Q^2. We conclude with a brief sketch of other potential ways to measure $\sin^2\theta_W$ in Section 6 and provide a future perspective and outlook in Section 7.

2. PAST MEASUREMENTS

In the following section, we review the three most precise published measurements of $\sin^2\theta_W$ at $Q^2 \ll M_Z^2$. The implications of the measurements for high- and low-scale dynamics are addressed in Section 4. A more comprehensive review of earlier experiments and associated developments can be found in Reference 55. A very recent review (55a) addresses a broader class of weak neutral-current observables.

2.1. Atomic Parity Violation in Cesium

One of the classic precision techniques in the field is the measurement of parity violation in atoms, as mentioned in Section 1. The electron–nucleus weak neutral-current interaction mediated by Z^0 exchange can be characterized by a new term in the Hamiltonian with an overall strength of $Q_W G_F$, and the weak charge Q_W is as defined in Equation 4. The new interaction induces a parity-violating matrix element $\mathrm{Im}(E1_{\mathrm{PNC}}) = Q_W k_{\mathrm{PNC}}/N$, where k_{PNC} is a quantity that can be computed from the atomic wave functions.

The experiment determines the ratio of $E1_{\mathrm{PNC}}$ to a Stark mixing matrix element $\mathrm{Im}(E1_{\mathrm{PNC}})/\beta$, where β is the vector transition polarizability. In 1997, the most precise result to date utilizing cesium was obtained (56): $\mathrm{Im}(E1_{\mathrm{PNC}})/\beta = 1.5935(56)\,\mathrm{mVcm}^{-1}$. The value of Q_W is obtained from

$$Q_W = \left(\frac{E1_{\mathrm{PNC}}/\beta}{M_{bf}/\beta}\right)\left(\frac{N\,M_{bf}}{k_{\mathrm{PNC}}}\right), \qquad 22.$$

where β and k_{PNC} were determined from atomic theory. In 1999, a more precise value of Q_W was extracted (57) on the basis of two improvements: M_{bf}/β was measured and β was obtained from a precise calculation of M_{bf}. Thereafter, the theoretical error in k_{PNC} was evaluated by benchmarking the calculation with other measurable quantities, such as hyperfine levels. With the improved data, researchers obtained $k_{\mathrm{PNC}} = 0.9065(36) \times 10^{-11} e a_0$. The new analysis gave the result $Q_W = -72.06\,(28)_{\mathrm{exp}}\,(34)_{\mathrm{theor}}$, which differed from the SM prediction by $2.3\,\sigma$.

Over the past decade, several theoretical developments (such as the inclusion of additional QED corrections and the Breit correction) seemed to resolve the discrepancy with the SM. The most detailed new corrections emerged from a new, high-precision calculation (58) that used the coupled cluster approximation and included triple excitations in addition to the single and double excitations that were treated in earlier calculations. The result was $k_{\mathrm{PNC}} = 0.8906(26) \times 10^{-11} e a_0$, which led to $Q_W(\mathrm{Cs})^{\mathrm{exp}} = -73.16(28)(20)$; this value is in excellent agreement with the SM expectation. However, a recent reevaluation (47) of some of the contributions has changed the result to $k_{\mathrm{PNC}} = 0.8977(40) \times 10^{-11} e a_0$, which is more consistent with results from earlier research

(59). This value leads to $Q_W = -72.58(43)$ and a value for $\sin^2\theta_W$, given in Equation 20, when compared with the latest theoretical prediction, including a small Pauli blocking correction (60). Indeed, with the inclusion of updated electroweak corrections, $Q_W(\mathrm{Cs})^{\mathrm{SM}} = -73.24(5)$, one expects a difference of 1.5 σ from experimental values. As discussed in Section 4, the result nevertheless continues to significantly constrain new TeV-scale lepton–quark interactions, thereby complementing direct collider searches.

2.2. SLAC E158

After the SLAC E122 experiment observed parity violation in neutral currents (discussed in Section 1), researchers considered the possibility of measuring parity violation in electron–electron (Møller) scattering. The value of A_{PV} in Møller scattering is proportional to $Q_W^e G_{\mathrm{F}} Q^2$ (61) and is highly suppressed. First, the electron's weak charge, $Q_W^e \approx -1 + 4\sin^2\theta_W$, is very small. Second, although sufficient luminosity can be generated by use of a very dense target, Q^2 for high-energy electrons scattering off electrons of mass m_e in a fixed target is $\sim m_e E_{\mathrm{beam}}$ and also very small. Although Q^2 can be increased by several orders of magnitude in collider mode, it is difficult to compensate for the larger loss in luminosity.

A feasible design concept was conceived (62) after the upgrade of the SLAC linear accelerator enabled high-intensity delivery of a 48-GeV beam for the SLAC Linear Collider. That development allowed the E158 experiment (48) to perform the first successful Møller A_{PV} measurement. However, even with a nearly 50-GeV beam, the predicted value of A_{PV} is only ~100 ppb. The production and monitoring of the highly polarized electron beam, in a high-luminosity target, required many technical developments; a novel spectrometer and detection techniques were also needed.

Below, we discuss the basic experimental technique for measuring A_{PV} in fixed-target polarized electron scattering. This discussion informs our description in Section 3 of future initiatives using the same technique.

The experiment was performed with 45- or 48-GeV polarized electrons in 100-ns bunches at a rate of 120 Hz. All electrons scattered from a 1.5-m-long hydrogen target with angles between 4.4 mrad and 7.5 mrad, and energies between 13 and 24 GeV were focused onto a copper and quartz fiber calorimeter by a quadrupole spectrometer. The helicity of the beam was reversed from pulse to pulse in a pseudorandom pattern by use of a Pockels cell to reverse the helicity of the laser, which produced the polarized electrons by photoemission from a strained GaAs crystal. The electron beam polarization was extracted via dedicated calibration runs that measured Møller scattering from a thin magnetized foil.

The researchers took care to eliminate false asymmetries due to, for example, differences in beam properties correlated with helicity. The position, angle, and energy of the beam were monitored with nanometer sensitivity, and small corrections were made on the basis of regular calibrations. Also, the asymmetry was reversed every few runs by insertion of a half-wave plate into the laser beam. Finally, the helicity of the beam was opposite for each of the two energies due to a $g-2$ precession in the magnets in the beam switchyard; therefore, the data were collected with roughly equal statistics at the two different beam energies (45 and 48 GeV). The asymmetry had the same magnitude and the correct sign for each of the four running configurations (half-wave plate state and beam energy), providing confidence in the results and suppressing a wide variety of possible small, spurious effects.

The result of the experiment was $A_{\mathrm{PV}} = -131 \pm 14\,(\mathrm{stat.}) \pm 10\,(\mathrm{syst.})$ ppb. The 3% shift in the running of $\sin^2\theta_W$ to low Q (mentioned in Section 1.3) caused (50) an ~40% shift in $Q_W^e = -1 + 4\sin^2\theta_W$. Indeed, the tree-level prediction for A_{PV} at the specific experimental

kinematics of E158 is ~250 ppb; the measured result unambiguously demonstrated the running of $\sin^2\theta_W$ (more than 6 σ) for the first time. The experiments took care to include full electroweak radiative corrections, including hard bremsstrahlung in the kinematic coverage (63), yielding the value of $\sin^2\theta_W$ quoted in Equation 19, which is currently the best measurement at $Q^2 \ll M_Z^2$. To extract a value for Q_W^e, it is first necessary to define it unambiguously; see Section 5 for a full discussion. A logical choice, similar to the case of APV discussed above, is to define Q_W^e in the static limit E and $Q^2 \to 0$. From the E158 result, the extracted value is $Q_W^e = -0.0369(52)$. In Section 4, we discuss the resulting limits on four-electron contact interactions and their complementarity to similar limits from lepton colliders.

2.3. NuTeV

The NuTeV experiment carried out the most precise measurement of neutrino neutral-current scattering by utilizing neutrino beams of high energy and purity produced from the 800-GeV proton beam at Fermilab. The weak mixing angle $\sin^2\theta_W$ was determined by measuring the ratios of neutral- to charged-current cross sections in DIS for both neutrinos (R_ν) and antineutrinos ($R_{\bar{\nu}}$) (49). By use of the ratios of cross sections, a major experimental uncertainty (the details of the composition of the neutrino beams) is largely canceled. The events were detected in an 18-m-long steel-scintillator calorimeter followed by an iron-toroid spectrometer. Because the target is approximately isoscalar, the parton distribution functions (PDFs) largely cancel in the ratio, reducing theoretical uncertainties.

A potential source of theoretical uncertainty in the extraction of $\sin^2\theta_W$ is the production of charm quarks via charged-current interactions with strange sea quarks. The PDF $s(\xi)$, where $\xi = x(1 + m_c^2/Q^2)$ is a slow-rescaling variable, must be used for the charged current, whereas $s(x)$ is used for the neutral current. However, by treating both R_ν and $R_{\bar{\nu}}$ as functions of m_c and $\sin^2\theta_W$, and combining both measurements, one can reduce the m_c error. In the simplest approximation, one can find a linear combination of R_ν and $R_{\bar{\nu}}$ that is independent of m_c and is proportional to $1 - 2(\sin^2\theta_W)$, the Paschos–Wolfenstein relation (64).

The published NuTeV result is nearly 3 σ away from the SM prediction, although some small shifts in either direction are expected from updates to the $K \to \pi e\nu$ branching ratio, radiative corrections, and isospin-breaking effects. Several phenomenological approaches exploring physics beyond the SM have been investigated to interpret the discrepancy; for a review, see, for example, Reference 65.

Many papers that attempt to explain the NuTeV result within the context of the SM have been published. One example invokes an asymmetric quark sea, parton-level charge–symmetry violation (CSV), and a modification of light-quark PDFs in the nuclear medium (the so-called isovector EMC effect) to bring the experimental results into perfect agreement with the SM (66). Other possibilities include radiative corrections (67) and nuclear shadowing (68, 69). Such corrections have not been formally incorporated into a reanalysis of the NuTeV result, because of concerns about the estimated theoretical uncertainties of various corrections. If CSV and the isovector EMC effect are indeed as large as given in Reference 66, it would be a significant discovery regarding fundamental QCD effects in nuclei. One of the auxiliary measurements in the proposed SoLID experiment, discussed in Section 3, would provide independent confirmation of this effect.

3. PARITY-VIOLATING ELECTRON SCATTERING

In this section, we describe the current experimental program of parity-violating electron scattering experiments. They are centered at two laboratories: the Thomas Jefferson National Accelerator

Facility (JLab) in Newport News, Virginia, and the Institut für Kernphysik at the University of Mainz, Germany. All the experiments described here make use of and build on the experimental techniques developed and improved since the pioneering SLAC E122 experiment took place; see Section 2.3 for an overview (in the description of SLAC E158).

CEBAF (the Continuous Electron Accelerator Facility) at JLab has been operating since 1995; it has a wide dynamic range in beam energy (from 1 to 6 GeV), beam current (a few nanoamperes to 180 μA), longitudinal beam polarization (>85%), and beam stability. An energy upgrade, which will be completed in 2014, will increase the maximum available beam energy to 12 GeV and will be capable of delivering 11 GeV at very high luminosity to existing experimental halls, significantly expanding the physics program (70). The Qweak and 6-GeV DIS experiments recently completed data collection, and two new initiatives, known as MOLLER and SoLID, have been proposed to utilize the 11-GeV beam after the completion of the energy upgrade project.

The Mainz Energy-recovering Superconducting Accelerator (MESA) is a new machine that has been approved for funding at Mainz. MESA offers 100 MeV in energy-recovery operation and 150–200 MeV for the conventional external beam mode (71). The latter mode will be used for the proposed P2 experiment. It is envisioned that the first beam will be available by the end of 2017.

3.1. Qweak

The Qweak experiment (72) was designed to measure the proton's weak charge, $Q_W^p \approx 1 - 4\sin^2\theta_W$, via $A_{\rm PV}$ in elastic electron–proton scattering. The experiment was first proposed in 2001 and constructed between 2006 and 2009; data collection was completed in 2012 in two run periods lasting a total of ∼11 months. Data analysis is ongoing, and final results are expected by 2014.

The experimental design centered around achieving $\delta(A_{\rm PV}) \approx \pm 2.1\%$ (stat.) and $\pm 1.3\%$ (syst.), resulting in $\delta(Q_W^p) \approx \pm 4\%$, and $\delta(\sin^2\theta_W) \approx \pm 0.3\%$. The incident beam energy was 1.165 GeV. Elastically scattered electrons in the range $\theta_{\rm lab} = 8 \pm 2^\circ \rightarrow \langle Q^2\rangle = 0.026$ GeV^2 were selected. The theoretical prediction at this Q^2 is $A_{\rm PV} \approx -230$ ppb, the piece proportional to $Q_W^p G_{\rm F}$ is −150 ppb, and the statistical goal is $\delta(A_{\rm PV}) \approx \pm 6$ ppb.

In Hall C at JLab, a 1-GeV 87%–longitudinally polarized electron beam, with a current of 150 to 180 μA, was incident on a 35-cm liquid hydrogen target capable of withstanding a heat load of 2.5 kW. Elastically scattered electrons were focused by the spectrometer/collimator system onto an azimuthally symmetric (with respect to the beam axis) arrangement of quartz bar–integrating Cherenkov detectors. The electron beam helicity was reversed in a quartet pattern at 960 Hz: A helicity state was chosen pseudorandomly at 240 Hz, and four consecutive pulses in a $(+--+)$ pattern or its complement were chosen accordingly. The width of the raw asymmetry distribution is a crucial benchmark; for Qweak, this width is 230 ppm for a quartet. The contribution from counting statistics is ∼200 ppm. The dominant sources of additional fluctuations were from detector resolution, target density fluctuations, and beam current monitor resolution.

Methods similar to those developed for SLAC E158 (Section 2.3) were employed to reduce the sensitivity of the measured asymmetry to helicity-correlated beam fluctuations. Also, a new method for reversing the relative direction between the spin and momentum vectors of the incident electrons before acceleration (the so-called double Wien filter) was employed every few weeks to gain further suppression. In addition to using Møller polarimetry every few days, Qweak used a Compton polarimeter that monitored the electron beam polarization continuously, concomitant with physics data collection; it is anticipated that the absolute beam polarization will be known to better than 1%. The absolute value of $\langle Q^2\rangle$ was calibrated in separate low-current runs by use of special-purpose drift chambers that could track individual scattered electrons.

3.2. MOLLER

The MOLLER experiment (73) is a new initiative proposed to measure A_{PV} in Møller scattering with an improvement of a factor of five in comparison to the E158 result. As discussed in Section 2.2, $A_{PV} \propto Q_W^e \approx -1 + 4\sin^2\theta_W$, which is reduced from its tree-level value by ∼40% due to radiative corrections. This measurement reduces the sensitivity of the extracted value of $\sin^2\theta_W$ to normalization errors, such as beam polarization, by an additional factor of two, compared with A_{PV} in elastic electron–proton scattering. The goal is a 2.3% measurement of Q_W^e that would result in $\delta(\sin^2\theta_W)_{stat} \approx 0.00025$, $\mathcal{O}(\pm 0.1\%)$—similar to the two best high-energy collider extractions of the parameter from measurements of Z^0 boson decays (Section 1).

The MOLLER design has many similarities to those of E158 and Qweak. An 11-GeV electron beam in JLab Hall A will be incident on a 1.5-m liquid hydrogen target. Use of a toroidal spectrometer would exploit the unique topology of Møller scattering involving identical particles, avoiding the typical 50% azimuthal acceptance loss associated with coil placement. This feat would be accomplished by employing an odd number of coils and collecting scattered electrons from both the forward and backward directions in the center-of-mass frame. The Møller scattered electrons in the full range of the azimuth would be directed to a ring focused 30 m downstream of the target. The detector system would incorporate a great deal of redundancy to monitor the principal backgrounds from electron–proton elastic and inelastic scattering to an accuracy of better than 1%. The prediction for A_{PV} is 35.6 ppb, and the statistical error goal is 0.74 ppb.

MOLLER will greatly benefit from the steady improvement in the techniques employed to measure parity-violating asymmetries to sub-parts-per-billion systematic precision and to achieve normalization control at the subpercent level. For example, two redundant continuous monitors of electron beam polarization would be employed to achieve 0.4% fractional accuracy. Auxiliary detectors would track individual particles at low rates to measure $\langle Q^2 \rangle$ to 0.5% fractional accuracy. Very forward angle detectors downstream of the main detectors would verify that luminosity fluctuations due to jitter in electron beam properties and target density are under control. All three methods to reverse the sign of the asymmetry that have been developed for previous experiments ($g-2$ spin flip, half-wave plate insertion, and the double Wien filter) would also be employed periodically. Technical design efforts for MOLLER are ongoing. The experimenters envision that funding approval will be obtained in 2013; construction of the apparatus may begin in 2015, which would allow commissioning by 2018, soon after full-luminosity beams become available at JLab.

3.3. Parity-Violating Deep-Inelastic Scattering at 6 GeV

The first measurement of A_{PV} in DIS since the original E122 measurement discussed in Section 1.1 (20) was carried out by JLab experiment E08011 (74). The primary motivation was to measure the poorly known neutral-current axial-vector quark couplings. The experiment ran in late 2009 with an incident beam energy of ∼6 GeV and Q^2 of ∼1–2 GeV^2; it collected sufficient statistics to measure A_{PV} off ^{2}H with a fractional accuracy better than 4%.

The scattered electrons were detected by the Hall A HRS (High Resolution Spectrometer) pair (75). Unlike other high-rate experiments discussed in this review, this experiment used a custom fast-counting data-acquisition system. Event-by-event particle identification was carried out at the hardware level with gas Cherenkov detectors and lead-glass shower counters. This information was fed into fast trigger logic to form electron and pion triggers that, in turn, were fed into scalers. The electron scaler results over the duration of each helicity time window of the electron beam were used to construct the raw asymmetry from which A_{PV} was extracted. The

electron trigger efficiency was greater than 95%, and the pion rejection ratio was greater than 1,000:1. Data analysis is ongoing, and final results are expected to be published by late 2013.

3.4. SoLID

The proposed SoLID experiment (76) at JLab aims to make a series of A_{PV} measurements with 0.5–1% fractional accuracy in DIS of electrons off ^{2}H. The primary motivation is to measure new linear combinations of neutral-current vector and axial-vector quark couplings with unprecedented accuracy, which would yield new and complementary access to new TeV-scale lepton–quark interactions, as well as a measurement of $\sin^2\theta_W$ with an uncertainty of $\delta(\sin^2\theta_W) \approx 0.0006$ at $Q \approx 2.5$ GeV.

The heart of the apparatus is a large-acceptance solenoid similar to those that have been used during the past four decades to provide the magnetic field inside collider detectors. This approach facilitates A_{PV} measurements in narrow x_{bj}, Q^2 bins: $0.3 \lesssim x_{bj} \lesssim 0.7$, with a lever arm of a factor of two in Q^2; $W^2_{min} > 4\,\text{GeV}^2$; and $\langle Q^2 \rangle \approx 5$ GeV^2. Such a large-volume and high-field solenoid ($\sim$1.5 T) is required to achieve sufficient statistics at the highest possible Q^2 and x_{bj}, provided that at least 50% azimuthal acceptance is obtained. It also facilitates shielding the detectors from target photons and sweeping out low-energy charged particles, while accommodating a significant target length and large laboratory scattering angles. The liquid deuterium target would be placed inside the solenoidal field, and several planes of absorbing material between the target and detectors with slits would tailor the momentum acceptance to the kinematic region of interest.

Importantly, unlike other A_{PV} measurements that integrate detector signals over different helicity periods, high-precision hit-based tracking with gas electron multiplier detectors is required to reconstruct the scattering angle and momentum of scattered electrons. To separate electrons from background, dominated by 100 times as many π^- particles as electrons, particle identification would be performed with heavy-gas Cherenkov detectors placed symmetrically about the beam axis inside the solenoid. An electromagnetic calorimeter would provide the primary electron trigger and allow additional pion rejection.

A proposal for the experiment was approved in January 2010 at JLab, and detailed simulations have been performed on the basis of the solenoid from the CLEO-II detector in the CESR e^+e^- storage ring. A significant research and development program has been launched to develop a detailed experimental design, and during the next few years the project will seek funding to run at JLab.

3.5. P2

The P2 experiment has been proposed for the newly funded MESA facility at Mainz. Its goal is $\delta(A_{PV}) = \pm 1.7\%$ (stat. + syst.) for elastic electron–proton scattering, which would yield $\delta(Q^p_W) \simeq 2\%$ and $\delta(\sin^2\theta_W) \pm 0.15\%$. Achieving these levels of precision would require a 200-MeV, 150-μA beam incident on a 60-cm liquid hydrogen target for 10,000 h. Apart from the improvement in statistical reach and, hence, sensitivity to New Physics over the JLab Qweak experiment, the lower beam energy would reduce theoretical uncertainties in extracting $\sin^2\theta_W$ (Section 5.3).

The design requires a solenoidal magnet (such as the inner tracking field of the ZEUS collider detector at DESY) downstream of the target. This magnet would focus scattered electrons within $10° < \theta_{lab} < 30°$ in the full range of the azimuth onto integrating Cherenkov detectors. The field would sweep out the large Møller electron background and allow judiciously placed annular slits to shield the detectors from the target's direct photon background. The theoretical prediction is $A_{PV} \approx 20$ ppb, and $\delta(A_{PV})$ (stat.) is ± 0.25 ppb. The total rate in the detectors would approach 0.5 THz.

Table 1 Models classified by chiral structure in the effective Lagrangian

Model	η^f_{LL}	η^f_{RR}	η^f_{LR}	η^f_{RL}
$LL^{\pm}$	± 1	0	0	0
$RR^{\pm}$	0	± 1	0	0
$LR^{\pm}$	0	0	± 1	0
$RL^{\pm}$	0	0	0	± 1
$VV^{\pm}$	± 1	± 1	± 1	± 1
$AA^{\pm}$	± 1	± 1	∓ 1	∓ 1
$VA^{\pm}$	± 1	∓ 1	± 1	∓ 1

The plus-sign and minus-sign superscripts indicate, respectively, constructive and destructive interference with the Standard Model.

The design must overcome many technical challenges, such as control over electron beam fluctuations at the subnanometer level and control over target density fluctuations to a few parts in 10^5. A new method to measure the electron beam polarization must be developed; such a method would require a novel polarized hydrogen gas target (77). The design and required research and development will be performed during the next few years, so the experiment would be ready to start commissioning when MESA first produces external beams (anticipated for 2017).

4. SENSITIVITY TO PHYSICS BEYOND THE STANDARD MODEL

In this section, we discuss the sensitivity of precision low-Q^2 measurements of weak neutral-current amplitudes to physics beyond the SM. We choose a few specific topics; many comprehensive reviews (29, 78) have studied aspects of the sensitivity to supersymmetric (79) as well as nonsupersymmetric (80) New Physics.

4.1. New Contact Interactions

If there is New Physics beyond the SM at some scale Λ above the electroweak scale, then in measurements at $Q^2 \ll \Lambda^2$ new dynamics can manifest themselves as small deviations from the expected SM rates. The new dynamics appear as contact interaction terms in an effective Lagrangian (81) that interfere with SM amplitudes. They can be parameterized as

$$\mathcal{L}_{\text{eff}} = \frac{g^2}{(1+\delta)\Lambda^2} \sum_{i,j=\text{L,R}} \eta^f_{ij} \bar{e}_i \gamma_\mu e_i \bar{f}_j \gamma^\mu f_j, \qquad 23.$$

summed over helicities [$\delta = 0(1)$ for $f = e$ ($f \neq e$)]. A typical convention sets $g^2/(4\pi) = 1$, and the $\eta^f_{ij} = \pm 1$ or 0. Precision measurements can then be translated into bounds on Λ. The effective Lagrangian in Equation 23 can be induced by a range of New Physics scenarios, such as low-scale quantum gravity with large extra dimensions, composite fermions, leptoquarks, and heavy Z' bosons, among others.

One can classify models that induce contact interactions according to the choices for the η^f_{ij}. **Table 1** shows a representative sample (82). Searches for such new contact interactions have been carried out in electron–positron, electron–proton, and hadron colliders.

The $LL^{\pm}$ model, shown in **Table 1**, is a benchmark scenario commonly used in contact interaction searches. For *eeqq*-type contact interactions, assuming quark-flavor independence, sensitive limits come from analyses of cross sections and asymmetries at LEP (83, 83a): $\Lambda^- > 8.0$ TeV

and $\Lambda^+ > 9.7$ TeV (95% CL). Similarly, $\Lambda^- > 7.0$ TeV and $\Lambda^+ > 4.5$ TeV were obtained for *eeee*-type contact interactions. More comprehensive bounds for several of the other models in **Table 1** can be found in Reference 84. More recently, the ATLAS Collaboration (85) derived bounds on the $LL^{\pm}$ model via measurements of fully inclusive Drell–Yan production in the di-electron channel, obtaining $\Lambda^- > 9.5$ TeV and $\Lambda^+ > 12.1$ TeV for the $LL^{\pm}$ *eeqq*-type contact interaction.

Low-Q^2 weak neutral-current measurements (discussed in Sections 2 and 3) can also probe contact interactions competitive with colliders. Specifically, the parity-violation measurements are sensitive to contact interactions of the form

$$\begin{aligned}\mathcal{L} = &-\frac{G_F}{\sqrt{2}}\sum_q \left[C_{1q}\bar{e}\gamma^\mu\gamma_5 e\bar{q}\gamma_\mu q + C_{2q}\bar{e}\gamma^\mu e\bar{q}\gamma_\mu\gamma_5 q\right] \\ &-\frac{G_F}{\sqrt{2}}C_{2e}\bar{e}\gamma^\mu\gamma_5 e\bar{e}\gamma_\mu e,\end{aligned} \qquad 24.$$

where the sum over q is over the quark flavors and the coefficients C_{1q}, C_{2q}, andC_{2e} are given by the sum of SM and new contact interaction contributions. Bounds on specific couplings can be translated into bounds on Λ. For example, the E158 measurement (Section 2.2) can be used to extract a value of the weak charge of the electron (in the static limit; see Section 5), $Q_W^e = 2C_{2e} \approx -1 + 4\sin^2\theta_W = -0.0369(52)$, compared with the SM prediction of $-0.0435(9)$. One can then extract 95%-CL limits on Λ by using

$$\Lambda \simeq \frac{2\sqrt{\pi}}{\sqrt{\sqrt{2}G_F\Delta Q_W^e}} \qquad 25.$$

to obtain $\Lambda^+_{LL} \geq 6.7$ TeV and $\Lambda^-_{LL} \geq 14.2$ TeV. Two observations are worth pointing out. First, the sensitivity is better than the limits from LEP, underscoring the power of measuring a small SM coupling such as $C_{2e}G_F$ to high precision. Second, the LEP limits come from measurements above W^+W^- threshold. The precise $\sin^2\theta_W$ measurements at the Z^0 resonance are not as sensitive to contact interaction amplitudes; the imaginary SM amplitude on top of the Z^0 resonance does not interfere with them. The proposed MOLLER measurement (Section 3.2) would improve these Λ limits to nearly 20 TeV, the best sensitivity to new flavor-conserving four-lepton contact interactions in existing facilities anywhere in the world. Better limits would require the construction of new facilities such as a linear collider, Z^0 factory, or neutrino factories, all of which are at least a decade away from fruition.

The chiral structures for *eeqq*-type contact interactions that appear in Equation 24 correspond to the $AV^{\pm}$ (C_{1i}) and $VA^{\pm}$ (C_{2i}) classes of models in **Table 1**. Limits on the $VA^{\pm}$ class of *eeqq*-type contact interactions shown in **Table 1** were obtained by the H1 (86) and ZEUS (87) experiments, which studied electron–proton and positron–proton collisions in the deep-inelastic regime to yield values of $\Lambda^- > 3.6$ TeV, $\Lambda^+ > 3.8$ TeV and $\Lambda^- > 3.2$ TeV, $\Lambda^+ > 3.3$ TeV, respectively.

A_{PV} and APV measurements in semileptonic reactions (discussed in Sections 2 and 3) have complementary and improved sensitivity. During the past 20 years, several experiments have measured A_{PV} in elastic electron–proton scattering at $0.1 < Q^2 < 1$ GeV^2 with the aim of constraining the strange quark form factors of the proton (88). Global fits to the data determined that the strange quark form factors were constrained to be small enough (89–91) that the low-Q^2 forward-angle data could then be analyzed to extract a measurement of $Q_W^p = 2(2C_{1u} + C_{1d})$. By expanding the parity-violating asymmetry at small scattering angles in powers of Q^2 with the parameterization $A_{PV} \propto Q_W^p + Q^2 B(Q^2)$, and then combining the results with the APV result on cesium discussed in Section 2.1 (which measures $C_{1u} + C_{1d}$), researchers obtained independent determinations of C_{1u} and C_{1d} (92). These determinations led to new constraints on the $AV^{\pm}$

Table 2 95%-CL reach of experiments[a] to the New Physics scale Λ ($g^2 = 4\pi$)

Experiment	Λ	Coupling
Cesium APV	9.9 TeV	$C_{1u} + C_{1d}$
E158	8.5 TeV	C_{ee}
Qweak	11 TeV	$2C_{1u} + C_{1d}$
SoLID	8.9 TeV	$2C_{2u} - C_{2d}$
MOLLER	19 TeV	C_{ee}
P2	16 TeV	$2C_{1u} + C_{1d}$

[a]Discussed in Sections 2 and 3. Abbreviation: APV, atomic parity violation.

chiral structure of ~3 TeV independently for *eeuu*- and *eedd*-type interactions; these constraints are comparable to the H1 and ZEUS limits.

The Qweak measurement (Section 3.1) will improve the sensitivity to the specific linear combination of $AV^{\pm}$ interactions $2C_{1u} + C_{1d}$ to better than 10 TeV, and the APV result on cesium already has a similar sensitivity reach for $C_{1u} + C_{1d}$. The SoLID measurement would be sensitive to a new linear combination of $VA^{\pm}$ *eeqq*-type contact interactions at the level of 8.9 TeV. Note that improvement of Λ sensitivity beyond 10 TeV in various chiral structures is necessary for a comprehensive search, as demonstrated by an example discussed at the end of the next section. **Table 2** summarizes the Λ reach and the specific coupling combinations of various experiments discussed in this review.

4.2. New Heavy Z' Bosons

Z' bosons with mass M'_Z in the TeV range appear in many extensions of the SM, including $SO(10)$, E_6, Little Higgs, and extradimensional theories. They arise from an additional $U(1)'$ gauge group that appears in such New Physics constructions. The phenomenology has been extensively reviewed (93, p. 537; 94), and the impact of precision electroweak data on a wide range of Z' models has been extensively analyzed (95, 96). Z' bosons have been constrained by electroweak precision data (95, 97), interference effects at LEP-II (84), and the Tevatron (98) with limits of ~1 TeV.

The simplest discovery mode for Z' bosons would be through an s-channel resonance in the dilepton or dijet topologies at colliders. The LHC will be able to explore the 1–5-TeV range of Z' boson masses, although the extraction of detailed properties such as the width and couplings will be difficult for $M'_Z \gtrsim 2$ TeV. In the region $M'_Z \lesssim 2$ TeV, a detailed study of the couplings will be enhanced by an analysis of off-peak LHC data and low-energy electroweak precision data. In such analyses, in which the interaction energies are well below the Z' boson mass ($M_{Z'}$), its exchange can be described by contact interactions wherein $\Lambda \approx M_{Z'}$. Constraints on contact interactions can then be translated into bounds on the mass and couplings of the Z' boson. For example, for Z' exchange between electrons and quarks, with the $LL^{\pm}$ chiral structure of **Table 1**, $M^2_{Z'}/(g^L_e g^L_q) \simeq \Lambda^2/(4\pi^2)$, where g^L_e and g^L_q are the left-handed Z' couplings to electrons and quarks, respectively.

Low-Q^2 A_{PV} measurements can be quite sensitive to Z' bosons due to their sensitivity to the interference between the electromagnetic amplitude and the Z' contact interaction. Furthermore, they probe different chiral combinations of Z' couplings compared with those at the LHC, thereby helping to remove degeneracies in parameter space in a purely LHC data–based analysis (99). In the context of exploring the reach of low-energy experiments, a class of E_6-based Z' models was

recently analyzed (100). Such Z' models arise from the spontaneous symmetry-breaking chain $E_6 \rightarrow SO(10) \times U(1)_\psi \rightarrow SU(5) \times U(1)_\chi \times U(1)_\psi \rightarrow \mathrm{SM} \times U(1)'$. The Z' bosons associated with the remaining $U(1)'$ can be written in the general form

$$Z' = \cos\alpha \cos\beta Z_\chi + \sin\alpha \cos\beta Z_Y + \sin\beta Z_\psi, \qquad 26.$$

where $Z_{\chi,Y,\psi}$ are gauge bosons associated with $U(1)_{\chi,Y,\psi}$ in the gauge eigenstate basis, β is the mixing angle between $U(1)_\chi$ and $U(1)_\psi$, and the angle α is nonvanishing in the presence of kinetic mixing between the $U(1)'$ and $U(1)_Y$ gauge groups. The angles α and β in Equation 26 provide a way to parameterize the class of E_6-based models. For example, the Z_χ, Z_ψ, and Z_η models correspond to α and $\beta = 0^0, 90^0$, and $-\arctan\sqrt{5/3}$, respectively. An example of how low-energy results and future initiatives discussed in this review complement collider searches is demonstrated in figure 1 of Reference 100, which shows excluded regions in the (α, β) parameter space for a hypothetical $M'_z = 1.2$ TeV.

A unique sensitivity of low-Q^2 A_{PV} measurements is with the so-called leptophobic Z' boson, which couples only to quarks and is thus difficult to discover at hadron colliders due to the irreducible QCD backgrounds. As mentioned in the previous section, measurements of the C_{2i} couplings by the proposed SoLID experiment (Section 3.4) will provide new sensitivity to $\mathrm{VA}^{\pm}$ *eeqq*-type contact interactions. Recently, the authors of References 101 and 102 pointed out that these couplings can be modified by a $\gamma - Z'$ vacuum polarization one-loop correction, thereby extending the current <100-GeV reach to 150–200 GeV.

4.3. Dark Parity Violation

Some recent New Physics scenarios have relatively light new degrees of freedom and hence cannot be classified in terms of contact interactions. The failure to observe such scenarios in high-energy experiments implies that such light particles must couple very weakly to SM particles. In certain regions of parameter space, low-energy precision experiments can have unique or enhanced sensitivity. In this context, another group (103, 104) recently investigated the possibility of a so-called dark Z boson, denoted Z_d and with mass m_{Z_d}, stemming from a spontaneously broken $U(1)_d$ gauge symmetry associated with a secluded dark particle sector. The Z_d boson can couple to the SM through a combination of kinetic and mass mixing with the photon and the Z^0 boson, with couplings ε and $\varepsilon_Z = \frac{m_{Z_d}}{m_Z}\delta$, respectively.

The original scenario with kinetic mixing with the photon was conjectured (105–108) to explain astrophysical observables as well as to account for the long-standing deviation of the muon's anomalous magnetic moment, a_μ, from SM expectations (109). If we take into account various experimental constraints, the a_μ discrepancy is naturally accommodated by kinetic mixing in the range

$$|\varepsilon| \simeq 2 \times 10^{-3} \quad 20\,\mathrm{MeV} \lesssim m_{Z_d} \lesssim 50\,\mathrm{MeV}. \qquad 27.$$

In the presence of mass mixing ($\delta \neq 0$), a new source of dark parity violation arises (103) such that it has a negligible effect at the Z^0 pole precision data but is quite discernible at low Q^2 through a shift in the weak mixing angle (104):

$$\Delta \sin^2\theta_W(Q^2) \simeq -0.42\,\varepsilon\delta\frac{m_Z}{m_{Z_d}}\left(\frac{m^2_{Z_d}}{Q^2 + m^2_{Z_d}}\right). \qquad 28.$$

In this scenario, the small (1.5-σ) APV deviation (discussed in Section 2.1), $\Delta \sin^2\theta_W(0) \simeq -0.003(2)$, suggests $\delta \simeq \pm 1 - 4 \times 10^{-3}$ as a potentially interesting region that can be explored by future APV or A_{PV} measurements, as we discuss further in the next section.

4.4. Weak Charges and New Physics

Employing the very precisely measured values of α, G_F, and m_Z along with m_t and $m_H = 126\,\text{GeV}$ in the one-loop corrected SM, but allowing for very heavy new particle loop effects via the electroweak precision S and T parameters (45, 110), leads to the predictions

$$\begin{aligned} m_W &= 80.362(6)\,\text{GeV}(1 - 0.0036S + 0.0056\,T), \\ \sin^2\theta_W(m_Z)_{\overline{\text{MS}}} &= 0.23124(6)(1 + 0.0157S - 0.0112\,T). \end{aligned} \qquad 29.$$

Comparison with experimental values yields $S = 0.06 \pm 0.08$ and $T = 0.10 \pm 0.09$, which can be used to significantly constrain models such as technicolor or the properties of fourth-generation fermions.

Similarly, the weak charges of particles and nuclei (defined at the static limit; E and $Q^2 = 0$) are precisely predicted at the loop level (26). However, in addition to S and T, deviations can be induced by New Physics in other ways. For example, Z' gauge bosons can cause $\mathcal{O}(m_Z^2/m_{Z'}^2)$ shifts in the weak charges similar to that observed in Equation 25 for generic contact interactions.

To illustrate relative sensitivities, we consider the Z_χ model of $SO(10)$, which violates parity in a well-specified manner (45, 111). Also, to allow New Physics differences between $\sin^2\theta_W(m_Z)_{\overline{\text{MS}}}$ and $\sin^2\theta_W(0)_{\overline{\text{MS}}}$ beyond SM running effects, we introduce $X(Q^2)$ (50, 112), which is similar to S but is Q^2 dependent. For heavy-particle loops [e.g., SUSY or heavy fermions (113)] with a generic mass scale M, where $X(Q^2) \approx \mathcal{O}(\alpha Q^2/M^2)$, X is already well constrained by the bounds on S from W and Z boson measurements. However, for very light New Physics such as the MeV-scale dark boson (Section 4.3) Z_d, which mixes with γ and Z^0 and thereby provides a new source of dark parity violation (103, 104), $X(Q^2) \propto m_{Z_d}^2/(Q^2 + m_{Z_d}^2)$ terms that are visible only in low $Q^2 \lesssim m_{Z_d}^2$ experiments can occur.

Given these New Physics scenarios, one finds the following shifts in the weak charges (45, 50, 60):

$$\begin{aligned} Q_W^e &= -0.0435(9)[1 + 0.25\,T - 0.34S + 0.7\,X(Q^2) + 7m_Z^2/m_{Z_\chi}^2], \\ Q_W^p &= 0.0707(9)[1 + 0.15\,T - 0.21S + 0.43\,X(Q^2) + 4.3m_Z^2/m_{Z_\chi}^2], \\ Q_W(^{12}\text{C}) &= -5.510(5)[1 - 0.003\,T + 0.016\,S - 0.033\,X(Q^2) - m_Z^2/m_{Z_\chi}^2], \\ Q_W(^{133}\text{Cs}) &= -73.24(5)[1 + 0.010\,S - 0.023\,X(Q^2) - 0.9m_Z^2/m_{Z_\chi}^2], \end{aligned} \qquad 30.$$

where the uncertainties have been somewhat expanded to account for as-yet-uncalculated higher-order effects. Several interesting features are apparent. The large ~40% radiative corrections to Q_W^e improve its fractional sensitivity to New Physics relative to Q_W^p. That makes Møller scattering better from a systematic (such as polarization) perspective but statistically similar in difficulty: $\delta(Q_W^e) \approx \pm 2\%$ is roughly equivalent to $\delta(Q_W^p) \approx \pm 1\%$. Both cases probe S and T below ± 0.1 and $m_{Z_\chi} \approx 2$ TeV.

For nuclei such as ^{12}C and ^{133}Cs, the T dependence is small (45). The assumption that $|S| \lesssim 0.1$ (based on existing constraints) suggests that they should be viewed as having mainly Z' and $X(Q^2)$ sensitivity. In the case of Z_χ, a $\pm 0.3\%$ measurement of $Q_W(^{12}\text{C})$ or $Q_W(^{133}\text{Cs})$ is roughly equivalent to $\delta(Q_W^e) \sim \pm 2\%$.

For $X(Q^2)$ effects such as those due to low-mass Z_d particles (103, 104, 107, 114) where $m_{Z_d} \approx 20 - 50$ MeV (discussed in the previous section), APV experiments in which Q^2 is naturally small ($Q^2 \ll m_{Z_d}^2$) are superior probes because they do not have the $m_{Z_d}^2/(Q^2 + m_{Z_d}^2)$ suppression. However, Q_W^e and Q_W^p are fractionally far more sensitive to $X(Q^2)$. For example, the $-0.9 \pm 0.6\%$ shift in the APV cesium result would lead to a 27% shift in Q_W^e if measured at the same Q. For $m_{Z_d} \approx 50$ MeV, the proposed MOLLER experiment ($Q \approx 75$ MeV) would provide an 8.4% shift

($\sim 3.7\sigma$). Below, we show that parity-violating electron scattering off ^{12}C may also be a good probe of parity-violating Z_d effects if low $\langle Q \rangle$ can be achieved.

5. SELECTED THEORETICAL ISSUES

5.1. Radiative Corrections to Parity-Violating Møller Scattering

The asymmetry $A_{\rm PV}$ in the Møller scattering process $e^- e^- \to e^- e^-$ (61) is a powerful probe of New Physics with relatively small theoretical uncertainties. In the mid 1990s, the proposed precision of the E158 measurement (Section 2.2) spurred the calculation of one-loop corrections, which shifts $A_{\rm PV}$ for Møller scattering by $\sim$40% (50). Indeed, given the plans to further improve the E158 measurement (the MOLLER proposal; see Section 3.2), there has been significant progress in controlling uncertainties in $A_{\rm PV}$ from higher-order radiative corrections at a level better than 1% (50, 53, 115–118). For $Q^2 \ll m_Z^2$, the tree-level expression is modified by radiative corrections as follows (50):

$$\begin{aligned} A_{\rm PV} = -\frac{\rho G_{\rm F} Q^2}{\sqrt{2}\pi\alpha} \frac{1-y}{1+y^4+(1-y)^4} \Bigg\{ & 1 - 4\kappa(0)\sin^2\theta_W(m_Z)_{\overline{\rm MS}} \\ & + \frac{\alpha(m_Z)}{4\pi\hat{s}^2} - \frac{3\alpha(m_Z)}{32\pi\hat{s}^2\hat{c}^2}(1-4\hat{s}^2)[1+(1-4\hat{s}^2)^2] \\ & + F_1(y, Q^2) + F_2(y, Q^2) \Bigg\}, \end{aligned} \tag{31.}$$

where $y = Q^2/s$, $\sqrt{s}$ is the center-of-mass energy, $\hat{s} \equiv \sin\theta_W(m_Z)_{\overline{\rm MS}}$, and $\hat{c} \equiv \cos\theta_W(m_Z)_{\overline{\rm MS}}$. The overall factor of $\rho = 1 + \mathcal{O}(\alpha)$ arises from radiative corrections (31, 50) to $G_{\rm F}$, which is defined through the muon decay process. The first and second terms in the second line of Equation 31 arise from WW and ZZ box diagram contributions, respectively. The WW box correction provides an $\sim$4% enhancement to the asymmetry. The ZZ box contribution, however, is suppressed by $(1-4\sin^2\theta_W)$ and gives only an $\sim$0.1% correction. The $F_1(y, Q^2)$ term (50) includes box, external leg, and vertex corrections involving at least one photon. The dominant effect, however, arises from the $\gamma - Z^0$ vacuum polarization and anapole moment contributions (**Figure 2**) that are encoded in $\kappa(0)$. The effective weak mixing angle at $Q^2 = 0$ in terms of the $\overline{\rm MS}$ value at the Z^0 pole is defined in terms of $\kappa(0)$ as

$$\sin^2\theta_W(0) = \kappa(0)\sin^2\theta_W(M_Z)_{\overline{\rm MS}}, \tag{32.}$$

corresponding to Equation 21 evaluated at $Q^2 = 0$. However, the experiment is conducted at finite Q^2, and the corresponding finite-Q^2 vacuum polarization effects are contained in $F_2(y, Q^2)$, which is very small (50).

A purely perturbative one-loop calculation gives

$$\begin{aligned} \kappa(0) = 1 - \frac{\alpha}{2\pi\hat{s}^2} \Bigg\{ & \frac{1}{3}\sum_f (T_{3f} Q_f - 2\hat{s}^2 Q_f^2) \ln\frac{m_f^2}{m_Z^2} \\ & - \left(\frac{7}{2}\hat{c}^2 + \frac{1}{12}\right)\ln\hat{c}^2 + \left(\frac{7}{9} - \frac{\hat{s}^2}{3}\right) \Bigg\}, \end{aligned} \tag{33.}$$

where the sum in the first line is over the quark and lepton flavors. However, at $Q^2 = 0$ the light-quark contribution to the $\gamma - Z^0$ vacuum polarization is nonperturbative and must be estimated using a dispersion relation that relates these effects to data on $e^+e^- \to$ hadrons. The result of such

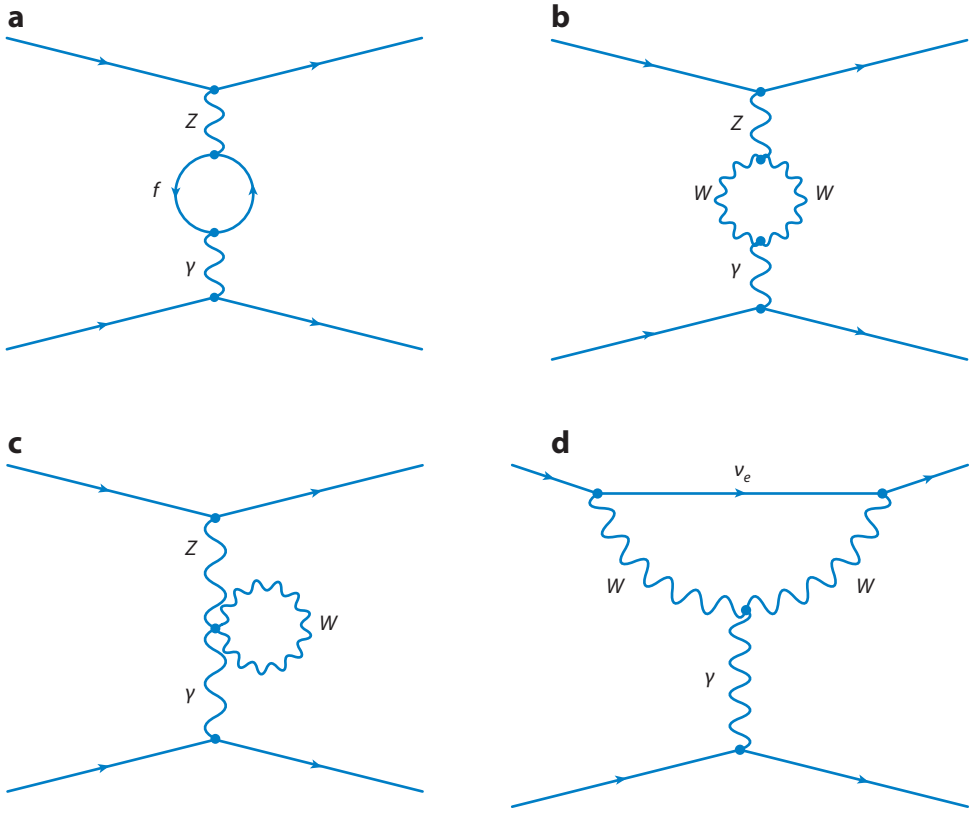

Figure 2

(*a–c*) $\gamma - Z$ mixing diagrams and (*d*) W-loop contribution to the anapole moment for parity-violating elastic electron scattering. Modified from Reference 52.

an analysis (36, 50, 119) leads to the replacement (for the quark contribution)

$$\frac{1}{3}\sum_f (T_{3f}Q_f - 2\hat{s}^2 Q_f^2)\ln\frac{m_f^2}{m_Z^2} \to -6.88 \pm 0.06 \qquad 34.$$

in Equation 33; the error in Equation 34 has been updated by the analysis presented in Reference 53, which we discuss in detail in the next section. It is these hadronic vacuum polarization effects that are primarily responsible for the large (∼40%) next-to-leading-order correction to the asymmetry. Coupled with anapole moment effects, they cause the effective weak mixing angle $\sin^2\theta_W(0)$ in Equation 32 to differ from $\sin^2\theta_W(m_Z)_{\overline{\rm MS}}$ by 3%. This discrepancy is referred to as the running from $Q^2 \approx m_Z^2$ to $Q^2 \ll m_Z^2$.

After accounting for the one-loop effects discussed above, one can now define the electron's weak charge, Q_W^e, in the limit E and $Q^2 \to 0$ as a static property of the electron, with the value quoted in Equation 30 for $m_H = 126$ GeV. Efforts to complete the full next-to-next-to-leading-order calculation of electroweak radiative corrections to the asymmetry are under way (120, 121). These corrections are expected to shift Q_W^e, possibly at the 1–2% level. Such efforts are essential in the context of the ultraprecise MOLLER proposal.

5.2. Running of the Weak Mixing Angle

An analysis similar to the one presented above must be carried out for any weak neutral-current experiment that aims to measure $\sin^2\theta_W$ at a level better than 1% at $Q^2 \ll m_Z^2$; one must carefully consider the dynamics that lead to the running of $\sin^2\theta_W$. In general, perturbative corrections enhanced by large logarithms of $\sim m_Z^2/Q^2$ (or m_Z^2/m_f^2, where m_f is some light fermion mass) can significantly affect a reliable interpretation of low-Q^2 measurements. For example, the ~40% reduction in the weak charge of the electron Q_W^e, and thus $A_{\rm PV}$ in Møller scattering (50), is due to the replacement (as discussed in Sections 1.3, 2.2, and 5.1)

$$1 - 4\sin^2\theta_W(m_Z)_{\overline{\rm MS}} \to 1 - 4\kappa(0)\sin^2\theta_W(m_Z)_{\overline{\rm MS}}. \qquad 35.$$

Here, $\kappa(0)$ encodes the radiative corrections from $\gamma - Z^0$ mixing and some anapole moment effects, motivating the definition of an effective weak mixing angle,

$$\sin^2\theta_W(0) \equiv \kappa(0)\sin^2\theta_W(m_Z)_{\overline{\rm MS}}, \qquad 36.$$

which simply corresponds to Equation 21 evaluated at $Q^2 = 0$. The quantity $\sin^2\theta_W(0)$ incorporates a set of universal radiative corrections that also affect other low-energy measurements, such as those from APV and Qweak. The perturbative one-loop result (50) for $\kappa(0)$ is given in Equation 33, and nonperturbative effects are incorporated by the replacement in Equation 34. Note that the one-loop result for $\kappa(0)$ contains large logarithms of m_Z^2/m_f^2 (at finite Q^2 there are also large logarithms of m_Z^2/Q^2) that can spoil convergence. Higher-precision extractions of $\sin^2\theta_W$ at low Q^2 require a resummation of such large logarithms, which brings the theory under better control and facilitates a more precise interpretation of measurements.

A well-known way to incorporate the resummation of large logarithms is to work in the $\overline{\rm MS}$ scheme for $\sin^2\theta_W$, as defined in Equation 8. This method uses a well-defined gauge-independent subtraction scheme to remove divergent terms arising in calculations of quantum corrections that use dimensional regularization. This subtraction scheme induces a logarithmic dependence on the renormalization scale μ, which is governed by a renormalization-group (RG) equation. Choosing $\mu^2 \approx Q^2$ of the process precludes the appearance of large logarithms in m_Z^2/Q^2. The $\overline{\rm MS}$ scheme also employs threshold matching to preclude large logarithms in m_Z^2/m_f^2 when $\mu \gg m_f$ or $\mu \ll m_f$. Crossing the particle-mass threshold from above, the corresponding particle is integrated out and the running below continues within an effective theory without this particle. These threshold matchings manifest themselves as discontinuities in the weak mixing angle running.

In the $\overline{\rm MS}$ scheme, the quantity of interest for low-energy experiments is $\sin^2\theta_W(0)_{\overline{\rm MS}}$, which corresponds to $\mu = 0$ in Equation 8. This quantity is defined in terms of the Z^0 pole value of the weak mixing angle as $\sin^2\theta_W(0)_{\overline{\rm MS}} = \kappa(0)_{\overline{\rm MS}}\sin^2\theta_W(m_Z)_{\overline{\rm MS}}$, where the quantity $\kappa(0)_{\overline{\rm MS}}$ is obtained by solving the RG equation between $\mu = m_Z$ and $\mu = 0$. More generally,

$$\sin^2\theta_W(Q^2)_{\overline{\rm MS}} = \kappa(Q^2,\mu)_{\overline{\rm MS}}\sin^2\theta_W(\mu^2)_{\overline{\rm MS}} \qquad 37.$$

gives the relation between the weak mixing angle at some fixed Q^2 in terms of its value at an arbitrary scale μ. Note that the product $\kappa(Q^2,\mu)_{\overline{\rm MS}}\sin^2\theta_W(\mu^2)_{\overline{\rm MS}}$ in Equation 37 is independent of the scale μ. This fact allows one to choose $\mu^2 = Q^2$ (along with threshold matching), effectively moving large logs from $\kappa(Q^2,\mu)_{\overline{\rm MS}}$ into $\sin^2\theta_W(\mu^2)_{\overline{\rm MS}}$ so that resummation can be performed using the RG evolution equation of $\sin^2\theta_W$. However, choosing $\mu^2 = m_Z^2$ introduces large logarithms of Q^2/m_Z^2 in $\kappa_{\overline{\rm MS}}(Q^2, \mu = m_Z)$, spoiling the convergence of perturbation theory. A solution to the RG equation of $\sin^2\theta_W(\mu)_{\overline{\rm MS}}$, for evolution between scales μ_0 and μ without crossing any

particle-mass thresholds, is (53)

$$\sin^2\theta_W(\mu)_{\overline{\rm MS}} = \frac{\alpha(\mu)_{\overline{\rm MS}}}{\alpha(\mu_0)_{\overline{\rm MS}}}\sin^2\theta_W(\mu_0)_{\overline{\rm MS}} + \lambda_1\left[1-\frac{\alpha(\mu)}{\alpha(\mu_0)}\right] + \frac{\alpha(\mu)}{\pi}\left[\frac{\lambda_2}{3}\ln\frac{\mu^2}{\mu_0^2} + \frac{3\lambda_3}{4}\ln\frac{\alpha(\mu)_{\overline{\rm MS}}}{\alpha(\mu_0)_{\overline{\rm MS}}} + \tilde{\sigma}(\mu_0) - \tilde{\sigma}(\mu)\right]. \quad 38.$$

In the above equation, $\lambda_{1,2,3}$ are numerical coefficients that take on different values depending on the range (μ_0, μ). This solution resums leading logs $\mathcal{O}(\alpha^n \ln^n \frac{\mu}{\mu_0})$, next-to-leading logs $\mathcal{O}(\alpha^{n+1} \ln^n \frac{\mu}{\mu_0})$ and $\mathcal{O}(\alpha\alpha_s^n \ln^n \frac{\mu}{\mu_0})$, next-to-next-to-leading logs $\mathcal{O}(\alpha\alpha_s^{n+1} \ln^n \frac{\mu}{\mu_0})$, and next-to-next-to-next-leading logs $\mathcal{O}(\alpha\alpha_s^{n+1} \ln^n \frac{\mu}{\mu_0})$. Nonperturbative effects arise from the contribution of light-quark loops in self-energy $\gamma - Z^0$ mixing diagrams when $\mu \approx \Lambda_{\rm QCD}$. These nonperturbative effects are incorporated in Equation 38 through the nonperturbative effects in the evolution of $\alpha(\mu)_{\overline{\rm MS}}$ and in the $\tilde{\sigma}(\mu_0)$, $\tilde{\sigma}(\mu)$ terms. These nonperturbative effects contribute an uncertainty in the extraction of $\sin^2\theta_W(0)_{\overline{\rm MS}}$ below the 10^{-4} level.

The value of $\sin^2\theta(0)_{\overline{\rm MS}}$, in terms of $\sin^2(m_Z)_{\overline{\rm MS}}$, can be obtained by use of Equation 38 combined with threshold matchings to evolve between the scales $\mu = m_Z$ and $\mu = 0$. The solution to the $\overline{\rm MS}$ RG evolution, expanded to one-loop order, is (53)

$$\kappa(0)_{\overline{\rm MS}} = \kappa(0) + \frac{2\alpha(m_Z)}{9\pi\hat{s}^2} = \kappa(0)^{\rm PT} = 1.03232 \pm 0.00029, \quad 39.$$

where nonperturbative effects have been included. The uncertainty has been improved by an order of magnitude compared with previous estimates. The quantity $\kappa(0)^{\rm PT}$ (54) is related to $\kappa(0)$ by the inclusion of additional so-called pinch terms of one-loop vertex and box graphs to make it process independent and intrinsically gauge invariant. In the $\overline{\rm MS}$ scheme, these additional pinch terms arise (53) from threshold matching corrections at $\mu = m_W$. Thus, working in the $\overline{\rm MS}$ scheme allows one to reproduce the known one-loop result and permits the inclusion of the leading higher-order corrections through resummation.

Figure 1 shows the running of $\sin^2\theta_W(Q^2)$ and $\sin^2\theta_W(Q^2)_{\overline{\rm MS}}$ for comparison. On the basis of the research described above and the prediction for $\sin^2\theta_W$ (discussed in Section 1) using fundamental SM input parameters, including m_H, we obtain

$$\sin^2\theta_W(m_Z)_{\overline{\rm MS}} = 0.23124(6) \rightarrow \sin^2\theta_W(0)_{\overline{\rm MS}} = 0.23871(9). \quad 40.$$

5.3. Weak Charge of the Proton

One can extract Q_W^p from the measurement of $A_{\rm PV}$ in electron–proton scattering. However, doing so requires considerations beyond the perturbative approach used for Møller scattering (Section 5.1). In particular, one must address hadronic physics that induces an energy dependence (122) to the $\gamma - Z^0$ box diagram (**Figure 3**). A definition of the weak charge that isolates such effects is (123)

$$A_{\rm PV} = -\frac{G_{\rm F}Q^2}{4\sqrt{2}\pi\alpha}\frac{W^{\rm PV}}{W^{\rm EM}}, \quad Q_W^p = \lim_{Q^2\rightarrow 0}\frac{W^{\rm PV}}{W^{\rm EM}}\bigg|_{E=0}, \quad 41.$$

where we write the asymmetry in terms of the general response functions $W^{\rm EM}$ and $W^{\rm PV}$, which depend on the electromagnetic and weak nucleon form factors. The conditions $E = 0$ and $Q^2 = 0$ in the definition of Q_W^p ensure that Q_W^p can be interpreted as a static property of the proton, independently of kinematics.

The tree-level SM value of $Q_W^p = 2(2C_{1u} + C_{1d}) = 1 - 4\sin^2\theta_W$, corresponding to the sum of the weak charges of the valence quarks in the proton, receives corrections from perturbative

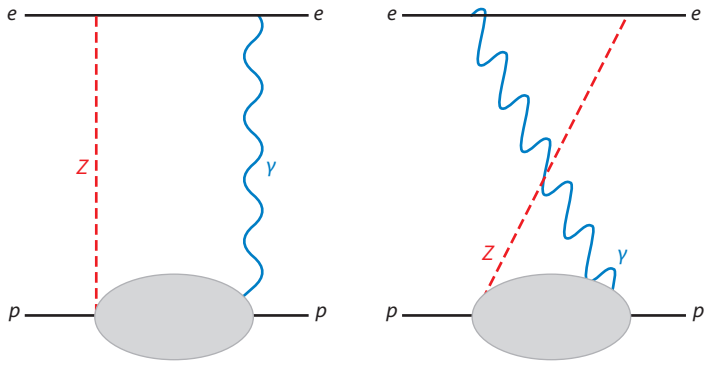

Figure 3

Box graphs contributing to $\Box_{\gamma Z}$ in elastic electron–proton scattering. Abbreviation: APV, atomic parity violation. Modified from Reference 122.

radiative effects and nonperturbative hadronic effects. The asymmetry $A_{\rm PV}$ can be written as

$$A_{\rm PV} = -\frac{G_{\rm F}Q^2}{4\sqrt{2}\pi\alpha}\left[\rho_{ep}[1-4\sin^2\theta_W(0)_{\overline{\rm MS}}] + {\rm Re}\,\Box_{WW} + {\rm Re}\,\Box_{ZZ} + {\rm Re}\,\Box_{\gamma Z}\right] - \frac{G_{\rm F}Q^2}{4\sqrt{2}\pi\alpha}B(Q^2), \qquad 42.$$

where $\rho_{ep} = 1 + \mathcal{O}(\alpha)$ incorporates radiative corrections (absorbing universal and process-dependent terms that are explicitly defined in equation 12 of Reference 123) due to the normalization of the weak neutral-current electron–proton amplitude relative to the charged-current muon decay amplitude used to define $G_{\rm F}$; $\Box_{WW}$, $\Box_{ZZ}$, and $\Box_{\gamma Z}$ are contributions from the two-boson box graphs in **Figure 3**. The remaining contribution, $B(Q^2)$, parameterizes proton structure at low Q^2 and vanishes in the forward limit [$B(Q^2) \to 0$ as $Q^2 \to 0$]. Comparing Equations 41 and 42 gives

$$Q_W^p = \left[\rho_{ep}(1-4\sin^2\theta_W(0)_{\overline{\rm MS}}) + {\rm Re}\,\Box_{WW} + {\rm Re}\,\Box_{ZZ} + {\rm Re}\,\Box_{\gamma Z}\right]\Big|_{E=0,Q^2\to 0}. \qquad 43.$$

All the box graphs appearing in Equation 42 are UV finite. The $\Box_{WW}$ and $\Box_{ZZ}$ box graphs (26, 119, 124) give to Q_W^p perturbative corrections of ∼26% and ∼3%, respectively, independently of the electron energy because loop momenta of order M_Z dominate. Remarkably, these corrections nearly cancel the reduction in Q_W^p due to the effect of $\kappa(0)$ (Equation 37), which makes it seem as though Q_W^p does not run with Q^2, in stark contrast to Q_W^e.

The calculation of the $\Box_{\gamma Z}$ contribution is more complicated because it is sensitive to small momentum scales and nonperturbative long-distance physics. Pinning down the size of the correction and theoretical uncertainty of the $\Box_{\gamma Z}$ contribution has been the subject of active research for almost three decades and continues today. This contribution can be written as the sum of two terms,

$$\Box_{\gamma Z} = \Box_{\gamma Z_{\rm A}} + \Box_{\gamma Z_{\rm V}}, \qquad 44.$$

corresponding to the Z^0 electron axial-vector ($g_{\rm A}^e$) and vector ($g_{\rm V}^e$) coupling contributions, respectively. The first calculation of $\Box_{\gamma Z}$ was carried out (26, 119) in the context of APV, where the electron energy $E \approx 0$. A cancellation between the box and crossed box graphs leads to a negligible

contribution from $\Box_{\gamma Z_A}$. The second and dominant contribution is

$$\mathrm{Re}\,\Box_{\gamma Z_V} = \frac{5\alpha(m_Z)_{\overline{\mathrm{MS}}}}{2\pi} g_V^e \left[\ln\frac{m_Z^2}{\Lambda^2} + C_{\gamma Z}(\Lambda)\right] \qquad 45.$$

suppressed by the weak vector coupling of the electron $g_V^e = 1 - 4\sin^2\theta_W(m_Z)_{\overline{\mathrm{MS}}}$. In Equation 45, $\Lambda \approx 1$ GeV is a hadronic cutoff that separates the perturbative and nonperturbative contributions. The first term arises from a perturbative contribution from loop momenta greater than Λ and the second term is the remaining nonperturbative contribution estimated to be $C_{\gamma Z}(\Lambda) = 3/2 \pm 1$ for $\Lambda = m_\rho$. This estimate was based on the Born approximation, in which the elastic proton intermediate state dominates the hadronic effects. The perturbative contribution in Equation 45 was recomputed (53, 124, 125), confirming the original result.

Recently, the $\Box_{\gamma Z}$ contribution was reexamined in the context of the kinematics of the Qweak experiment (122). This study showed that there is a contribution, which was not considered in previous analyses, that grows with the incident electron energy. In the forward limit $Q^2 \to 0$, a dispersion relation relates the real and imaginary parts of the $\Box_{\gamma Z}$ contribution as

$$\begin{aligned}\mathrm{Re}\,\Box_{\gamma Z_A}(E) &= \frac{2E}{\pi}\int_{\nu_\pi}^{\infty}\frac{d\nu'}{\nu'^2 - E^2}\mathrm{Im}\,\Box_{\gamma Z_A}(\nu'),\\ \mathrm{Re}\,\Box_{\gamma Z_V}(E) &= \frac{2}{\pi}\int_{\nu_\pi}^{\infty}\frac{\nu' d\nu'}{\nu'^2 - E^2}\mathrm{Im}\,\Box_{\gamma Z_V}(\nu'),\end{aligned} \qquad 46.$$

and the imaginary parts are given in terms of the parity-violating DIS $\gamma - Z$ interference structure functions $F_{1,2,3}^{\gamma Z}(x, Q^2)$ as (122, 123, 126, 127)

$$\begin{aligned}\frac{\mathrm{Im}\,\Box_{\gamma Z_A}}{\alpha g_A^e} &= \int_{W_\pi^2}^{s}\frac{dW^2}{(s-M^2)^2}\int_0^{Q^2_{\max}}\frac{dQ^2}{1+\frac{Q^2}{M_Z^2}}\left[F_1^{\gamma Z} + \frac{s(Q^2_{\max}-Q^2)}{Q^2(W^2-M^2+Q^2)}F_2^{\gamma Z}\right],\\ \frac{\mathrm{Im}\,\Box_{\gamma Z_V}}{-\alpha g_V^e} &= \int_{W_\pi^2}^{s}\frac{dW^2}{(s-M^2)^2}\int_0^{Q^2_{\max}}\frac{dQ^2}{1+\frac{Q^2}{M_Z^2}}\left[\frac{2(s-M^2)}{W^2-M^2+Q^2} - 1\right]F_3^{\gamma Z}.\end{aligned} \qquad 47.$$

Here, $x = Q^2/(2p\cdot q)$, $W^2 = (p+q)^2$, $W_\pi^2 = (M + m_\pi)$, $\nu_\pi = (W_\pi^2 - M^2)/(2M)$, $Q^2_{\max} = (s-M^2)(s-W^2)/s$, and p is the initial proton momentum. The explicit overall factor of the electron energy E in $\mathrm{Re}\,\Box_{\gamma Z_A}$, shown in Equation 46, is the origin of the new electron energy dependence in $\Box_{\gamma Z}$. Note that although the $\Box_{\gamma Z_V}$ contribution is suppressed by g_V^e, no such suppression exists for $\Box_{\gamma Z_A}$, which yields a significant energy-dependent correction to the Qweak asymmetry.

As shown by Equations 46 and 47, estimating the size of the $\Box_{\gamma Z}$ contribution requires knowledge of the $F_{1,2,3}^{\gamma Z}$ structure functions over a wide range of kinematics. This range can be classified into three regions: (*a*) elastic ($W^2 = M^2$), (*b*) resonance ($W_\pi^2 \le W^2 \lesssim 4$ GeV^2), and (*c*) deep inelastic ($W^2 > 4$ GeV^2). Note that because $Q^2 = 0.026$ GeV^2 in Qweak, the structure functions cannot be expressed in terms of the leading-twist PDFs, as is usually done when $Q^2 \gg \Lambda^2_{\mathrm{QCD}}$. A combination of data and modeling of the structure functions is necessary in the three regions for an accurate estimate of $\Box_{\gamma Z}$. Moreover, the dispersion relations in Equation 46 were derived in the forward limit, leading to an additional Q^2 dependence in the box graphs mentioned above; this dependence was found (123) to be small.

There have been several recent estimates (122, 123, 126–128) of the size of the $\Box_{\gamma Z}$ contribution and its associated uncertainty in determining Q_W^p. Although this is still an active area of research and there are some differences between approaches and results, the general consensus is that $\Box_{\gamma Z}$ contributes an ∼5–6% correction for $E_{\mathrm{beam}} \approx 1$ GeV that must be subtracted to determine Q_W^p, as defined in Equation 43, with an $\sim 2-3\%$ uncertainty; the anticipated experimental uncertainty is

4%. The larger of the uncertainty estimates has a contribution from model dependence associated with flavor rotations. Auxiliary measurements from current and future JLab experiments discussed in this review will cover a wider range of $F_{1,2,3}^{\gamma Z}$ and further reduce the theoretical uncertainty in $\Box_{\gamma Z_A}$. The theoretical uncertainty is already negligible for the P2 proposal (Section 3.5), with $E_{\text{beam}} \approx 0.2$ GeV.

6. OTHER POTENTIAL FUTURE MEASUREMENTS

6.1. Atomic Parity Violation

Several new APV projects are under way. Two separate initiatives on heavier atoms are being pursued to take advantage of the greatly enhanced parity-violating amplitudes at higher values of Z. At TRIUMF in Canada, an experiment to use francium atoms (129) is being designed, and at KVI in the Netherlands, Ra^+ ions (130) are being investigated. In both designs, chains of isotopes could be measured such that the atomic theory uncertainties cancel when ratios of different isotopes are taken. However, note that the measurement of Q_W for a single isotope, properly normalized to the atomic theory, will remain important because it has rather different sensitivities to New Physics effects. Indeed, there are often scenarios in which New Physics effects also tend to cancel when isotope ratios are taken. There are also plans to measure isotope chains in dysprosium and ytterbium (131), although the atomic theory is more challenging. These measurements will also be sensitive to the thickness of the radius of the neutron distribution, which is a subject of considerable interest in itself (132).

6.2. Neutrino Scattering

Currently, the NuTeV deep-inelastic neutrino scattering result (Equation 20) represents the best neutrino determination of the weak mixing angle ($\sim \pm 0.7\%$). It differs by nearly 3 σ from SM expectations; this situation requires resolution. The advent of future high-intensity neutrino sources, designed primarily for neutrino oscillation studies, could in principle resolve the NuTeV anomaly. For example, a fine-grained near detector at the Fermilab LBNE facility has been suggested as a means of achieving $\pm 0.2\%$ sensitivity at Q^2 values similar to that of NuTeV (133).

Low-energy neutrino sources, such as nuclear power reactors, spallation neutron sources, and β beams, used in conjunction with very massive detectors could measure $\sin^2\theta_W(m_Z)_{\overline{\text{MS}}}$ at very low $\langle Q \rangle (\sim 1 - 30)$ MeV by using ν_e and ν_μ scattering on electrons. Fractional sensitivities of $\pm 1\%$ on $\sin^2\theta_W$ appear to be feasible. Unfortunately, reaching the $\pm 0.1\%$ goal appears very challenging both statistically and systematically. Nevertheless, it is a well-motivated goal because at that level of accuracy, the measurements probe many interesting varieties of New Physics (134–138).

6.3. Parity-Violating Electron Scattering off ^{12}C

More than 20 years ago, a measurement (139) in $\vec{e} - {}^{12}\text{C}$ elastic scattering of $A_{\text{PV}}(e\text{C}) \propto G_{\text{F}} Q^2 \sin^2\theta_W$ at the MIT-Bates laboratory achieved $\pm 25\%$ precision. Along the way, researchers developed techniques that set the stage for parity-violating electron scattering experiments of the type discussed in this review.

Today, higher electron currents with better longitudinal polarization, combined with a much larger acceptance spectrometer (140), could improve the statistical figure of merit by 10^4, making an asymmetry measurement of $Q_W(^{12}\text{C})$ to $\pm 0.3\%$ statistically feasible. The means to control the sources of spurious false asymmetries at the level required have been developed and are similar to those of other proposed A_{PV} measurements. However, the control of normalization errors and

especially the measurement of the electron beam polarization will require detailed study. Assuming that a total $\pm 0.3\%$ determination of $Q_W(^{12}\mathrm{C})$ is possible, what can we learn, in comparison with other A_{PV} measurements, from such an effort?

With reference to the discussion in Section 4.4 and Equation 30 in particular, we pointed out that, in terms of m_{Z_χ} sensitivity, a total uncertainty of $\pm 0.3\%$ in the measurement of $Q_W(^{12}\mathrm{C})$ is roughly equivalent to the future MOLLER proposal to determine $Q_W(e)$ to $\pm 2.3\%$. It also represents an improvement of a factor of approximately three over $Q_W(\mathrm{Cs})$, in which there is a 1.5-σ difference between theory and experiment.

Perhaps another compelling motivation for a new ultraprecise $Q_W(^{12}\mathrm{C})$ measurement comes from the sensitivity to a light Z_d dark gauge boson (103, 104), introduced in Section 4.3. Indeed, explaining the $(g-2)_\mu$ 3.6-σ discrepancy with 20 MeV $\lesssim m_{Z_d} \lesssim$ 50 MeV and $\varepsilon \approx 2 \times 10^{-3}$ $\gamma - Z_d$ mixing, as well as accommodating the 1.5-σ discrepancy in Q_W (Cs), requires an $X(Q^2)$ corresponding to

$$\Delta \sin^2\theta_W(Q^2) \approx -0.003(2)\frac{m_{Z_d}^2}{Q^2+m_{Z_d}^2}. \qquad 48.$$

Compare this value with the ± 0.0007 experimental sensitivity of a $\pm 0.3\%$ $A_{\mathrm{PV}}(^{12}\mathrm{C})$ measurement.

At the MESA facility in Mainz, such a measurement could be performed by use of the same concept as that for the P2 proposal (Section 3.5). With the projected technical capabilities for other proposed A_{PV} initiatives, a series of three simultaneous $\pm 0.3\%$ measurements with $100 \lesssim Q \lesssim 150$ MeV at $E_{\mathrm{beam}} \approx 200$ MeV and a second series of $\pm 0.4\%$ measurements with $60 \lesssim Q \lesssim 100$ MeV at $E_{\mathrm{beam}} \approx 140$ MeV could be considered. Although the statistics would be achievable in two 1-year runs, the systematic control of normalization errors merits a detailed study.

Achieving a lower Q than 60 MeV would be challenging without new experimental technologies. Nevertheless, a program of measurements could become quite compelling, depending on the results of ongoing A_{PV} and dark matter initiatives, or if the 50–100-MeV mass range for Z_d becomes important to explore. Together, a factor-of-three overall improvement, compared with the existing cesium APV measurement, and the low-Q^2 sensitivity to $X(Q^2)$ and dark Z_d effects may be enough to motivate a new, much higher sensitivity $A_{\mathrm{PV}}(^{12}\mathrm{C})$ program.

6.4. Weak Mixing Angle at an Electron–Ion Collider

The design of a new experimental facility known as the Electron–Ion Collider (EIC) is under study as the next logical step in the study of QCD in nuclear matter (141). One operational mode will involve high-energy collisions between highly polarized electrons and polarized ^{1}H, ^{2}H, and ^{3}He with $20 \lesssim \sqrt{s} \lesssim 150$ GeV and luminosity of $\sim 10^{33-34}\,\mathrm{cm}^2\,\mathrm{s}^{-1}$. The collider environment and the envisioned hermetic detector package at high luminosity will allow for precision A_{PV} measurements over a wide kinematic range with little uncertainty from limited knowledge of PDFs and negligible impact of higher-twist effects.

By mapping A_{PV} as a function of Q^2 and the fractional energy loss of the scattered electron y (something that is very challenging to do in fixed-target experiments), a clean separation of two linear combinations of couplings, namely $2C_{1u} - C_{1d}$ and $2C_{2u} - C_{2d}$, will become feasible as a function of Q^2. Thus, at the highest luminosities and center-of-mass energies envisioned at the EIC, very precise measurements of these combinations can be achieved at a series of Q^2 values, allowing for a series of precision $\sin^2\theta_W$ extractions. **Figure 4** shows the projected uncertainties on the weak mixing angle extracted from such a data set (142) for a center-of-mass energy of 140 GeV and an integrated luminosity of 200 fb^{-1}.

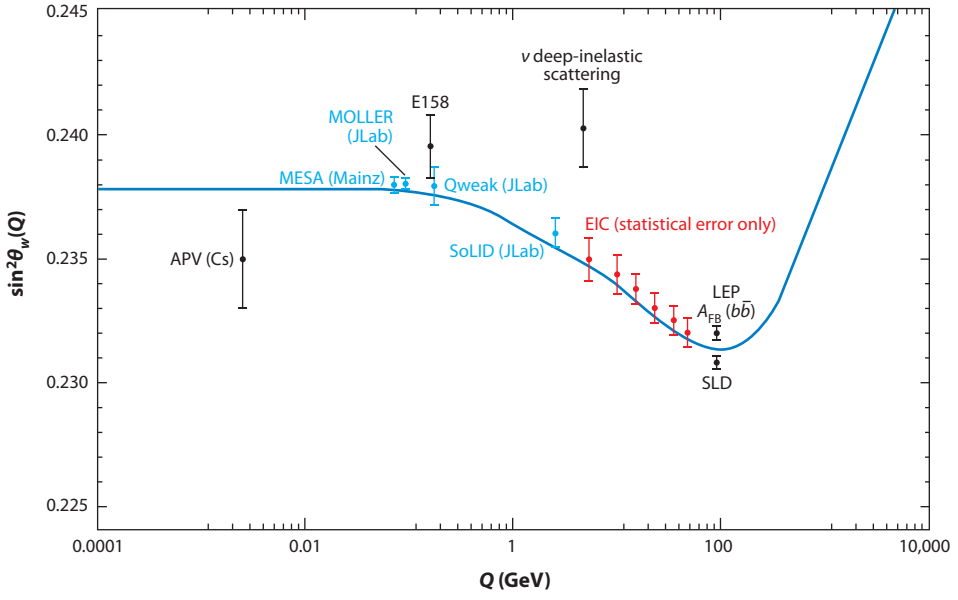

Figure 4

Current and future $\sin^2\theta_W$ measurements. The black points are published results discussed in Section 2, the blue points are projections for projects discussed in Section 3, and the red points are projected data for the Electron–Ion Collider (EIC) at $\sqrt{s} = 140$ GeV and 200 fb^{-1}. Abbreviation: APV, atomic parity violation.

7. SUMMARY AND OUTLOOK

Precision measurements of electroweak parameters have played an important role in confirming the SM and probing for New Physics effects. The recent (tentative) discovery of the Higgs boson at the LHC, with $m_H \approx 126$ GeV, completes the elementary particle spectrum of the minimal SM and allows for even more refined predictions and comparisons between theory and experiment.

Already, determinations of m_W and $\sin^2\theta_W(m_Z)_{\overline{\rm MS}}$ (at the Z^0 pole) are testing SM expectations at a level better than $\pm 0.1\%$; so far, no glaring evidence of discrepancies has been found [although m_W is somewhat high and $\sin^2\theta_W(m_Z)_{\overline{\rm MS}}$ measurements have a broader spread than one would like]. These tests confirm the SM at its quantum-loop level and constrain New Physics appendages to it; examples include fourth-generation fermions, technicolor, supersymmetry, and GUTs.

Low-Q^2 SM observables, such as weak neutral-current charges Q_W, can also be precisely computed and compared with measurements. Results from classic measurements, such as those from cesium APV and SLAC E158, are currently at approximately the $\pm 0.5 - 1\%$ sensitivity level for $\sin^2\theta_W(Q^2 \approx 0)$. At that level, they test quantum loops and confirm the anticipated running of $\sin^2\theta_W(Q^2)$ by $\sim 3\%$ as it evolves from $Q^2 \approx 0$ to m_Z^2. In addition, those measurements play a special role in constraining Z' bosons, leptoquark models, and generic four-fermion contact interactions.

There is rich physics in the radiative corrections that leads, for example, to the remarkable numerical difference between the electron and proton renormalized weak charges. This difference has implications for the design, feasibility, and systematic error propagation of precision experiments. It also emphasizes the value of studying the SM with high precision in as many reactions as possible. A priori, one cannot know where New Physics—physics that can be described

at low energies by new contact interactions or physics that appears in vacuum polarization or box diagrams at the quantum-loop level—may be observed.

Now, a new generation of polarized electron scattering experiments is on the horizon. The Qweak experiment at JLab has completed data collection and is in the analysis stage. It will improve the low-Q^2 determination of $\sin^2\theta_W(Q^2)$ to $\pm 0.3\%$ with little theoretical uncertainty, given the recent advances in the evaluation of γZ^0 box diagrams. We will soon see whether the result presents any surprises.

The tremendous technical advances in experimental methods, as well as the theoretical advances in precision calculations, have set the stage for very low Q^2 electron–electron and electron–proton asymmetry measurements that will aim for an unprecedented $\pm 0.1\%$ $\sin^2\theta_W(Q \approx 0)$ sensitivity, allowing them to be competitive with the best Z^0 pole studies. At that level, Z' models and contact interactions are probed at mass scales in the 1–20-TeV range, the running of $\sin^2\theta_W(Q^2)$ is precisely verified, or dramatically new phenomena may be uncovered. For example, low-Q^2 measurements may unveil so-called dark parity violation due to a very light, weakly coupled Z_d boson from the dark matter sector. If so, such a discovery would revolutionize the focus of low-energy parity-violation experiments and would provide strong motivation for other challenging low- and high-energy experiments designed to shed new light on dark physics. Surprises advance science, but they are possible only if we push the boundaries of our abilities.

DISCLOSURE STATEMENT

The authors are not aware of any affiliations, memberships, funding, or financial holdings that might be perceived as affecting the objectivity of this review.

ACKNOWLEDGMENTS

We thank J. Erler, Y. Li, and M. Ramsey-Musolf for useful discussion and input on figures. Our research has been funded in part by the US Department of Energy under grants DE-FG02-88R40415-A018 (K.K.), DE-AC02-98CH10886 (W.J.M.), and DE-FG02-84ER40146 (P.A.S.) and by the US National Science Foundation under grant NSF-PHY-0705682 (S.M.). W.J.M. acknowledges partial support as a fellow in the Gutenberg Research College.

LITERATURE CITED

1. Glashow S. *Nucl. Phys.* 22:579 (1961)
2. Weinberg S. *Phys. Rev. Lett.* 19:1264 (1967)
3. Higgs PW. *Phys. Lett.* 12:132 (1964)
4. Higgs PW. *Phys. Rev. Lett.* 13:508 (1964)
5. Higgs PW. *Phys. Rev.* 145:1156 (1966)
6. Englert F, Brout R. *Phys. Rev. Lett.* 13:321 (1964)
7. Guralnik G, Hagen C, Kibble T. *Phys. Rev. Lett.* 13:585 (1964)
8. Bouchiat C, Iliopoulos J, Meyer P. *Phys. Lett. B* 42:91 (1972)
9. 't Hooft G. *Nucl. Phys. B* 35:167 (1971)
10. Hasert F, et al. (Gargamelle Neutrino Collab.) *Phys. Lett. B* 46:138 (1973)
11. Bollini C, Giambiagi J, Sirlin A. *Nuovo Cim. A* 16:423 (1973)
12. Marciano W. *Nucl. Phys. B* 84:132 (1975)
13. Bouchiat M, Bouchiat C. *J. Phys.* 35:899 (1974)
14. Lewis L, et al. *Phys. Rev. Lett.* 39:795 (1977)
15. Baird P, et al. *Phys. Rev. Lett.* 39:798 (1977)

16. Barkov L, Zolotorev M. *J. Exp. Theor. Phys. Lett.* 27:357 (1978)
17. Conti R, et al. *Phys. Rev. Lett.* 42:343 (1979)
18. Bucksbaum P, Commins E, Hunter L. *Phys. Rev. Lett.* 46:640 (1981)
19. Bouchiat M, Guena J, Hunter L, Pottier L. *Phys. Lett. B* 117:358 (1982)
20. Prescott C, et al. *Phys. Lett. B* 77:347 (1978)
21. Georgi H, Glashow S. *Phys. Rev. Lett.* 32:438 (1974)
22. Georgi H, Quinn HR, Weinberg S. *Phys. Rev. Lett.* 33:451 (1974)
23. Marciano WJ. *Phys. Rev. D* 20:274 (1979)
24. Marciano WJ, Senjanovic G. *Phys. Rev. D* 25:3092 (1982)
25. Marciano W, Sirlin A. *Phys. Rev. Lett.* 46:163 (1981)
26. Marciano WJ, Sirlin A. *Phys. Rev. D* 29:945 (1984)
27. Aoyama T, Hayakawa M, Kinoshita T, Nio M. *Phys. Rev. Lett.* 109:111807 (2012)
28. Tishchenko V, et al. (MuLan Collab.) arXiv:1211.0960 [hep-ex] (2012)
29. Beringer J, et al. (Part. Data Group) *Phys. Rev. D* 86:010001 (2012)
30. Sirlin A. *Phys. Rev. D* 22:971 (1980)
31. Marciano W, Sirlin A. *Phys. Rev. D* 22:2695 (1980)
32. Marciano W, Sirlin A. *Conf. Proc. C* 810424:151 (1981)
33. Gambino P, Sirlin A. *Phys. Rev. D* 49:1160 (1994)
34. Abe K, et al. (SLD Collab.) *Phys. Rev. Lett.* 84:5945 (2000)
35. ALEPH Collab., et al. arXiv:1012.2367 [hep-ex] (2010)
36. Marciano WJ. In *Spin Structure in High Energy Processes: Proceedings*, ed. L DePorcel, C Dunwoodie, p. 35. Stanford, Calif.: Stanford Univ. Press (1993)
37. Ferroglia A, Ossola G, Passera M, Sirlin A. *Phys. Rev. D* 65:113002 (2002)
38. Awramik M, Czakon M, Freitas A, Weiglein G. *Phys. Rev. D* 69:053006 (2004)
39. Awramik M, Czakon M, Freitas A. *J. High Energy Phys.* 0611:048 (2006)
40. Marciano WJ. arXiv:hep-ph/0411179 (2004)
41. Marciano WJ. arXiv:hep-ph/0003181 (2000)
42. Aad G, et al. (ATLAS Collab.) *Phys. Lett. B* 716:1 (2012)
43. Chatrchyan S, et al. (CMS Collab.) *Phys. Lett. B* 716:30 (2012)
44. Ferroglia A, Sirlin A. arXiv:1211.1864 [hep-ph] (2012)
45. Marciano WJ, Rosner JL. *Phys. Rev. Lett.* 65:2963 (1990)
46. Marciano WJ. *J. Phys. Conf. Ser.* 312:102002 (2011)
47. Dzuba V, Berengut J, Flambaum V, Roberts B. *Phys. Rev. Lett.* 109:203003 (2012)
48. Anthony PL, et al. (SLAC E158 Collab.) *Phys. Rev. Lett.* 95:081601 (2005)
49. Zeller G, et al. (NuTeV Collab.) *Phys. Rev. Lett.* 88:091802 (2002)
50. Czarnecki A, Marciano WJ. *Phys. Rev. D* 53:1066 (1996)
51. Czarnecki A, Marciano WJ. *Int. J. Mod. Phys. A* 13:2235 (1998)
52. Czarnecki A, Marciano WJ. *Int. J. Mod. Phys. A* 15:2365 (2000)
53. Erler J, Ramsey-Musolf MJ. *Phys. Rev. D* 72:073003 (2005)
54. Ferroglia A, Ossola G, Sirlin A. *Eur. Phys. J. C* 34:165 (2004)
55. Musolf MJ, et al. *Phys. Rep.* 239:1 (1994)
55a. Erler J, Su S. *Prog. Part. Nucl. Phys.* 71:119 (2013)
56. Wood C, et al. *Science* 275:1759 (1997)
57. Bennett S, Wieman CE. *Phys. Rev. Lett.* 82:2484 (1999)
58. Porsev S, Beloy K, Derevianko A. *Phys. Rev. D* 82:036008 (2010)
59. Dzuba V, Flambaum V, Ginges J. *Phys. Rev. D* 66:076013 (2002)
60. Blunden P, Melnitchouk W, Thomas A. *Phys. Rev. Lett.* 109:262301 (2012)
61. Derman E, Marciano WJ. *Ann. Phys.* 121:147 (1979)
62. Kumar KS, Hughes E, Holmes R, Souder P. *Mod. Phys. Lett. A* 10:2979 (1995)
63. Kolomensky Y, Shumeiko N, Suarez J, Zykunov V. *Int. J. Mod. Phys. A* 20:7365 (2005)
64. Paschos E, Wolfenstein L. *Phys. Rev. D* 7:91 (1973)
65. Davidson S, et al. *J. High Energy Phys.* 0202:037 (2002)
66. Bentz W, Cloet I, Londergan J, Thomas A. *Phys. Lett. B* 693:462 (2010)

67. Diener KP, Dittmaier S, Hollik W. *Phys. Rev. D* 72:093002 (2005)
68. Hirai M, Kumano S, Nagai TH. *Phys. Rev. D* 71:113007 (2005)
69. Brodsky SJ, Schmidt I, Yang JJ. *Phys. Rev. D* 70:116003 (2004)
70. Dudek J, et al. *Eur. Phys. J. A* 48:187 (2012)
71. Aulenbacher K, et al. *ICFA Beam Dyn. Newslett.* 58:145 (2012)
72. Armstrong D, et al. arXiv:1202.1255 [physics] (2012)
73. Mammei J. (MOLLER Collab.) *Nuovo Cim. C* 035N04:203 (2012)
74. Zheng X. (JLab Hall A Collab.) *Nuovo Cim. C* 035N04:72 (2012)
75. Alcorn J, et al. *Nucl. Instrum. Methods A* 522:294 (2004)
76. Souder P. (SoLID Collab.) *AIP Conf. Proc.* 1441:123 (2012)
77. Chudakov E, Luppov V. *IEEE Trans. Nucl. Sci.* 51:1533 (2004)
78. Ramsey-Musolf MJ. *Phys. Rev. C* 60:015501 (1999)
79. Ramsey-Musolf M, Su S. *Phys. Rep.* 456:1 (2008)
80. Chang WF, Ng JN, Wu JM. *Phys. Rev. D* 79:055016 (2009)
81. Eichten E, Lane KD, Peskin ME. *Phys. Rev. Lett.* 50:811 (1983)
82. Kroha H. *Phys. Rev. D* 46:58 (1992)
83. Schael S, et al. (ALEPH Collab.) *Eur. Phys. J. C* 49:411 (2007)
83a. Schael S, et al. (ALEPH Collab., DELPHI Collab., L3 Collab., OPAL Collab., LEP Electroweak Work. Group) arXiv:1302.3415 [hep-ex] (2013)
84. LEP Collab., et al. arXiv:hep-ex/0412015 (2004)
85. Aad G, et al. (ATLAS Collab.) *Phys. Rev. D* 87:015010 (2013)
86. Aaron F, et al. *Phys. Lett. B* 705:52 (2011)
87. Chekanov S, et al. (ZEUS Collab.) *Phys. Lett. B* 591:23 (2004)
88. Kumar KS, Souder P. *Prog. Part. Nucl. Phys.* 45:S333 (2000)
89. Young RD, Roche J, Carlini RD, Thomas AW. *Phys. Rev. Lett.* 97:102002 (2006)
90. Liu J, McKeown RD, Ramsey-Musolf MJ. *Phys. Rev. C* 76:025202 (2007)
91. González-Jiménez R, Caballero J, Donnelly T. arXiv:1111.6918 [nucl-th] (2011)
92. Young RD, Carlini RD, Thomas AW, Roche J. *Phys. Rev. Lett.* 99:122003 (2007)
93. Rizzo TG. arXiv:hep-ph/0610104 (2006)
94. Langacker P. *Rev. Mod. Phys.* 81:1199 (2009)
95. Erler J, Langacker P, Munir S, Rojas E. *J. High Energy Phys.* 0908:017 (2009)
96. Erler J, Langacker P, Munir S, Rojas E. *J. High Energy Phys.* 1111:076 (2011)
97. del Aguila F, de Blas J, Perez-Victoria M. *J. High Energy Phys.* 1009:033 (2010)
98. CDF Collab., D0 Collab., Jaffre M. *Proc. Sci.* EPS-HEP2009:244 (2009)
99. Li Y, Petriello F, Quackenbush S. *Phys. Rev. D* 80:055018 (2009)
100. Erler J, Langacker P, Munir S, Rojas E. arXiv:1108.0685 [hep-ph] (2011)
101. Buckley MR, Ramsey-Musolf MJ. *Phys. Lett. B* 712:261 (2012)
102. González-Alonso M, Ramsey-Musolf MJ. arXiv:1211.4581 [hep-ph] (2012)
103. Davoudiasl H, Lee HS, Marciano WJ. *Phys. Rev. D* 85:115019 (2012)
104. Davoudiasl H, Lee HS, Marciano WJ. *Phys. Rev. Lett.* 109:031802 (2012)
105. Holdom B. *Phys. Lett. B* 166:196 (1986)
106. Fayet P. *Phys. Rev. D* 70:023514 (2004)
107. Bouchiat C, Fayet P. *Phys. Lett. B* 608:87 (2005)
108. Pospelov M. *Phys. Rev. D* 80:095002 (2009)
109. Bennett G, et al. (Muon $g-2$ Collab.) *Phys. Rev. D* 73:072003 (2006)
110. Peskin ME, Takeuchi T. *Phys. Rev. Lett.* 65:964 (1990)
111. London D, Rosner JL. *Phys. Rev. D* 34:1530 (1986)
112. Maksymyk I, Burgess C, London D. *Phys. Rev. D* 50:529 (1994)
113. Kurylov A, Ramsey-Musolf M, Su S. *Phys. Rev. D* 68:035008 (2003)
114. Davoudiasl H, Lee HS, Marciano WJ. *Phys. Rev. D* 86:095009 (2012)
115. Denner A, Pozzorini S. *Eur. Phys. J. C* 7:185 (1999)
116. Petriello FJ. *Phys. Rev. D* 67:033006 (2003)
117. Aleksejevs A, Barkanova S, Ilyichev A, Zykunov V. *Phys. Rev. D* 82:093013 (2010)

118. Aleksejevs A, et al. arXiv:1010.4185 [hep-ph] (2010)
119. Marciano W, Sirlin A. *Phys. Rev. D* 27:552 (1983)
120. Aleksejevs A, et al. *Phys. Rev. D* 85:013007 (2012)
121. Aleksejevs A, et al. arXiv:1202.0378 [hep-ph] (2012)
122. Gorchtein M, Horowitz C. *Phys. Rev. Lett.* 102:091806 (2009)
123. Gorchtein M, Horowitz C, Ramsey-Musolf MJ. *Phys. Rev. C* 84:015502 (2011)
124. Erler J, Kurylov A, Ramsey-Musolf MJ. *Phys. Rev. D* 68:016006 (2003)
125. Musolf M, Holstein BR. *Phys. Lett. B* 242:461 (1990)
126. Sibirtsev A, Blunden P, Melnitchouk W, Thomas A. *Phys. Rev. D* 82:013011 (2010)
127. Rislow BC, Carlson CE. *Phys. Rev. D* 83:113007 (2011)
128. Blunden P, Melnitchouk W, Thomas A. *Phys. Rev. Lett.* 107:081801 (2011)
129. Aubin S, et al. *AIP Conf. Proc.* 1441:555 (2012)
130. Giri G, et al. *Can. J. Phys.* 89:69 (2011)
131. Tsigutkin K, et al. *Phys. Rev. Lett.* 103:071601 (2009)
132. Sil T, Centelles M, Vinas X, Piekarewicz J. *Phys. Rev. C* 71:045502 (2005)
133. Mishra S, Petti R, Rosenfeld C. *Proc. Sci.* NUFACT08:069 (2008)
134. Marciano WJ, Parsa Z. *J. Phys. G* 29:2629 (2003)
135. Conrad J, Link J, Shaevitz M. *Phys. Rev. D* 71:073013 (2005)
136. Rosner JL. *Phys. Rev. D* 70:037301 (2004)
137. de Gouvêa A, Jenkins J. *Phys. Rev. D* 74:033004 (2006)
138. Agarwalla SK, Huber P. *J. High Energy Phys.* 1108:059 (2011)
139. Souder P, et al. *Phys. Rev. Lett.* 65:694 (1990)
140. Souder P, Holmes R. In *Proceedings of the Pasadena Workshop on Parity Violation in Electron Scattering*, ed. EJ Beise, RD McKeown, p. 137. Teaneck, N.J.: World Sci. (1990)
141. Deshpande A, et al. arXiv:1212.1701 [nucl-ex] (2012)
142. Boer D, et al. arXiv:1108.1713 [nucl-th] (2011)

Annual Review of Nuclear and Particle Science

Volume 63, 2013

Contents

Index

Errata

An online log of corrections to *Annual Review of Nuclear and Particle Science* articles may be found at http://nucl.annualreviews.org/errata.shtml